QUARTERLY JOURNAL
OF THE
ROYAL METEOROLOGICAL SOCIETY

Vol. 115 APRIL 1989 No. 487

Q. J. R. Meteorol. Soc. (1989), **115**, pp. 425–461 551.515.41:551.558.1

Observed structure of mesoscale convective systems and implications for large-scale heating

By ROBERT A. HOUZE, Jr.

Department of Atmospheric Sciences, University of Washington, Seattle, Washington, U.S.A.

(Received 22 December 1987; revised 11 October 1988)

SUMMARY

Mesoscale convective cloud systems that produce large amounts of rain in mid-latitudes and most of the rain in the tropics consist of a combination of convective and stratiform cloud. The convective regions contain numerous deep cells that are often but not always arranged in lines. The stratiform region is an outgrowth of the convective ensemble; it lies adjacent to the convective region and is seeded by ice particles detrained from convective towers. Sometimes it lies to the rear of a propagating convective line, while on other occasions it surrounds the convection.

The heating of the large-scale environment by a mesoscale convective system is affected by both the convective and stratiform regions. Although processes such as melting and radiation are important, the net heating by a system is dominated by condensation and evaporation associated with vertical air motions. This paper reviews recent observational evidence regarding the mean vertical motion profiles in the convective and stratiform regions of mesoscale convective systems and the implications of these mean motions for the vertical distribution of heating of the large-scale environment.

In both the convective and the stratiform regions, vertical motions have been determined by various techniques, including composites of rawinsonde and aircraft wind data, single- and dual-Doppler precipitation radar analyses, and wind-profiler observations. In stratiform regions, these data consistently show mean vertical velocity that is upward in the upper troposphere and downward in the lower troposphere. The level separating upward from downward motion is located from 0 to 2 km above the 0 °C level, depending on location within the stratiform region. Diagnostic calculations show that these vertical motion profiles imply heating of the upper troposphere and cooling of lower levels by stratiform-region processes.

Data on vertical motions in the convective regions are less consistent from case to case. These data sometimes indicate that the mean vertical velocity in convective regions is maximum in the lower troposphere. In other cases, the data indicate a maximum in the high troposphere. Diagnostic calculations show that heating profiles diagnosed from these two types of profile are quite different, the first having a maximum of heating in the lower troposphere, while the second has a maximum in the middle troposphere. Although it is difficult to determine whether or not the differences in estimates arise from different types of observations, analysis methods or sampling strategies, it seems likely that they stem from differences in the large-scale environment of the different mesoscale systems.

The ubiquitous occurrence of stratiform regions in mesoscale convective systems and hurricanes together with their consistent heating profiles, which systematically concentrate heating in upper levels while cooling lower levels, are a major consideration in evaluating the interaction of mesoscale systems with the large-scale environment. However, the consistency of the stratiform profiles from case to case indicates that the variability of net (convective plus stratiform) heating profiles from case to case lies primarily in the variation of the convective-region profiles from one case to another. It is suggested that future work should focus on the convective-region vertical profiles of vertical motion and heating and on the large-scale environmental factors that may control the variation of these profiles from case to case.

1. INTRODUCTION

The heating of the large-scale environment by deep cumulonimbus convection is one of the more important intriguing and elusive problems of the atmosphere. Throughout the tropics, where energy is put into the atmosphere, deep cumulonimbus clouds are the

agents by which high energy air is conveyed from the planetary boundary layer to the upper troposphere (Riehl and Malkus 1958). Similar vertical transports accompany outbreaks of deep convection in mid-latitudes. However, the manner in which the deep convection interacts with the large-scale environment during the vertical transport and exactly how the heating of the large-scale atmosphere that occurs during this process is distributed in the vertical remain rather poorly documented and understood. It seems evident that these interactions and the concomitant vertical distribution of heating are important. With simple linear global models it has been shown that the global circulation is sensitive to specified vertical distributions of heating associated with tropical convection (e.g. Hartmann *et al.* 1984; DeMaria 1985). However, general circulation and numerical weather prediction models ultimately must determine internally the location and nature of the convection to which the large-scale flow in turn responds. To test whether such models are predicting convective heating processes correctly, some empirical information is needed regarding the actual vertical distribution of heating by deep convection in representative atmospheric settings.

With this goal in mind, Houze (1982) summarized the cloud and precipitation structure of mesoscale convective systems (MCSs) as observed in the tropical field experiments GATE and MONEX, and he estimated the vertical distribution of diabatic heating associated with an idealized MCS. He further showed that synoptic-scale vertical motions diagnosed from GATE rawinsonde data seemed to correspond to the vertical distribution of heating estimated for the idealized tropical cloud system. However, Houze's (1982) idealized tropical MCS was based primarily on studies of radar reflectivity measurements and satellite imagery obtained in GATE and MONEX. Since his paper, many more data sets from these and other field projects, including some in mid-latitudes, have been examined. The purpose of this paper is to reassess the tenets and conclusions of Houze (1982) in light of these recent studies. Specifically, three aspects of the Houze paper will be re-examined.

First, the idealized model will be reviewed and updated in section 2.

Second, the extent of the applicability of the idealized conceptual model that he used to derive his conclusions will be examined. The key aspect of this model is that the precipitation of the MCS is divisible into clearly identifiable convective and stratiform regions, within which sharply differing vertical distributions of diabatic heating prevail. The recent studies alluded to above have borne out this structure, not only in various types of tropical MCSs, but in mid-latitude convection and hurricanes. Section 3 of this paper will review recent observations that illustrate the broad applicability of the conceptual model.

The third aspect of Houze's study to be re-examined here is the vertical distribution of vertical air motion within the idealized MCS. In determining the vertical distributions of diabatic heating in the convective and stratiform regions of the idealized MCS, Houze associated the rainfall in the convective region with vertical profiles of mass transport that must have occurred during the precipitation process. A similar procedure was followed for the stratiform region. Thus the magnitudes of vertical mass transport in the convective and stratiform regions were scaled appropriately according to the rain amounts in each region. However, assumptions had to be made about the water budgets of the convective and stratiform regions and about the vertical profiles of vertical motion in each region. The convective-region profile was estimated using a one-dimensional weakly entraining jet cumulus model. The vertical motion profile for the stratiform region was based primarily on indirect thermodynamic evidence, presented in studies such as those of Zipser (1969, 1977) and Houze (1977). Since 1982, several studies have documented the vertical motion profiles in the convective and stratiform regions more directly—in

some cases by composite analysis of rawinsonde and aircraft wind data, in other cases by Doppler radar observations. Section 4 of this paper reviews the data now available on the vertical distribution of vertical air motion in the convective and stratiform regions of MCSs and examines whether these distributions are consistent with the vertical distributions of heating estimated by Houze (1982).

2. Review of conceptual model

(*a*) *Idealized cloud system structure*

The structure and lifecycle of Houze's (1982) idealized tropical MCS are depicted in Fig. 1. In its mature stage (Fig. 1(b)) the cluster consists partly of convective towers, which contain buoyant updraughts, negatively buoyant downdraughts and heavy showers of rain. In addition, lighter precipitation extends over a horizontal distance of 100–200 km. It falls from a deep stratiform cloud extending from the mid-troposphere to the top of the cirrus shield.

Houze (1989) has added detail to the conceptual model by describing aspects of the relationship between the deep convective cells and the associated stratiform region. His schematic (Fig. 2) emphasizes microphysical and kinematic aspects of the precipitation processes in the convective and stratiform regions. Precipitation ice is generated as growing drops are carried up past the 0 °C level by the convective updraughts. Thereafter the ice particles grow by riming as they accrete supercooled cloud drops forming in the updraught at mid-to-upper levels. Although some of these particles become quite heavy and fall out rapidly as part of the convective rain, others become only moderately dense and fall more slowly ($\approx$1 m/s). These more slowly falling particles are spread laterally through the stratiform cloud region by the horizontal wind as they drift downward. The detrainment of the snow from the convective cells is thus the mechanism by which precipitating ice particles are introduced into the stratiform portion of the cloud system.

In Fig. 2, the most intense radar bright band and the heaviest stratiform rain at the surface occur where the convectively generated snow particles reach the 0 °C level, after their passage through the stratiform cloud (Smull and Houze 1985; Rutledge and Houze 1987). In this environment of widespread but moderate vertical motion, the snow particles drift downward while growing by vapour deposition. In the layer between 0 and −12 °C, the particles aggregate to form large snowflakes (Houze and Churchill 1987) and apparently sometimes grow by riming as well (Leary and Houze 1979b). Rutledge and MacGorman (1988) note that the riming in this layer plays a role in the electrification of the stratiform region of mid-latitude MCSs.

From diagnostic modelling of the water budget and microphysical processes in a stratiform region similar to those in tropical rain systems, Rutledge and Houze (1987) found that both the influx of snow into the stratiform region from the convective cells and the growth of the snow as it passed through the region of the mesoscale updraught contributed strongly to the stratiform precipitation process. Without the lateral influx of snow, their model stratiform cloud was incapable of producing significant rain. On the other hand without the mesoscale ascent within the stratiform cloud, only about one fourth as much stratiform rain reached the surface. Thus, the deep convective cells seed the stratiform cloud with snow generated in the convection, but mean ascent in the stratiform region leads to a large increase in the mass of precipitating condensate through vapour deposition—a process in which a large amount of latent heat is released.

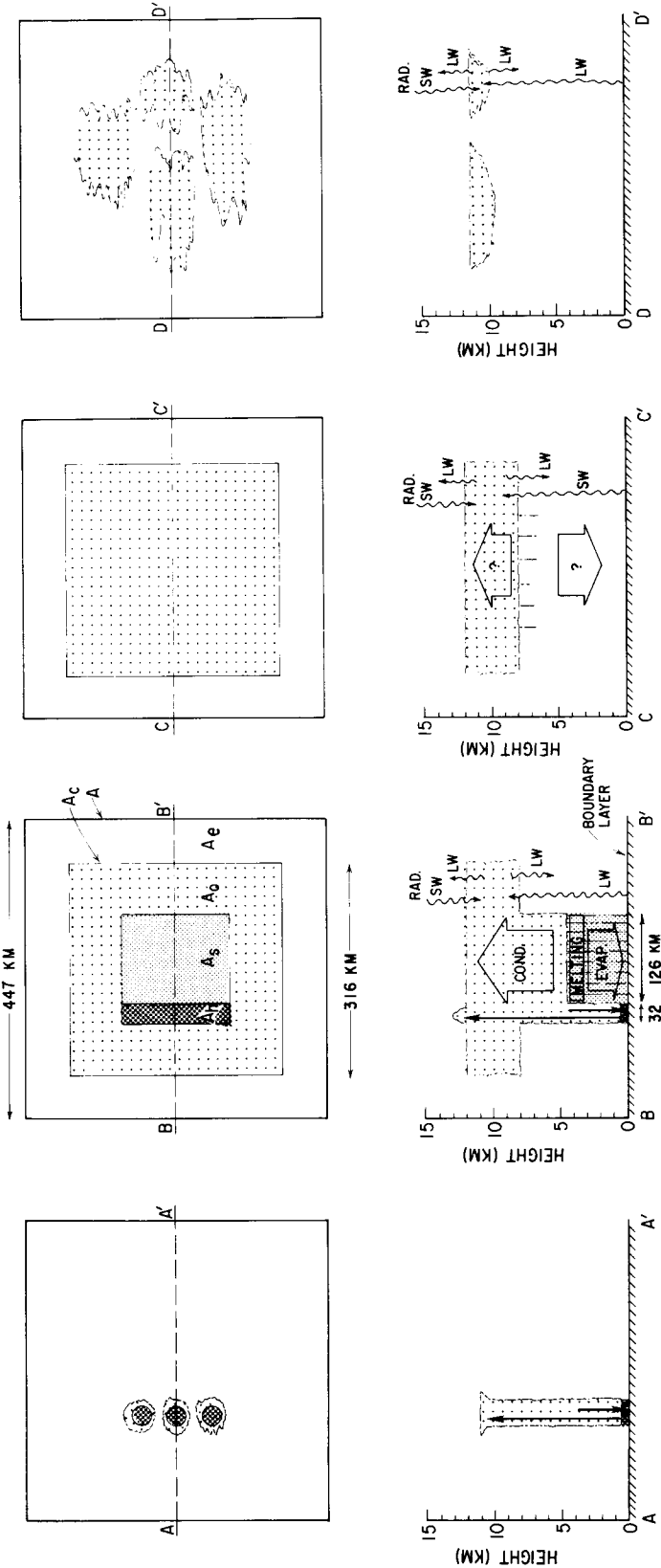

Figure 1. Schematic of a tropical cloud cluster in four successive stages of development. (a) Early stage in which cluster consists of isolated precipitating convective towers. (b) Mature stage in which a cloud shield has developed and covers A_c, convective cells are located in area A_h, stratiform precipitation is falling from a middle-level cloud base within area A_s, and an area A_o is covered by upper-level cloud overhang. (c) Weakening stage in which convective cells have disappeared, stratiform precipitation remains, and upper cloud is becoming thin and breaking up. (d) Dissipating stage in which no precipitation remains and upper cloud is becoming thin and breaking up. In (a) and (b), cumulus-scale updraughts and downdraughts are denoted by straight solid arrows. In (b) and (c), mesoscale updraught and downdraught are shown by wide, open arrows; condensation (COND) in the mesoscale updraught, evaporation (EVAP) in the mesoscale downdraught, and the melting layer in the stratiform precipitation region are indicated. Question marks indicate that the existence of the mesoscale draughts in stage (c) is uncertain. Shortwave (SW) and longwave (LW) radiation (RAD) are denoted by wavy arrows. The upper panels of (a) and (d) are plan views. The lower panels are vertical sections along the indicated horizontal line segments. Area A is a large-scale region containing the cloud cluster, and A_e is a cloud-free environmental area surrounding the cluster (from Houze 1982).

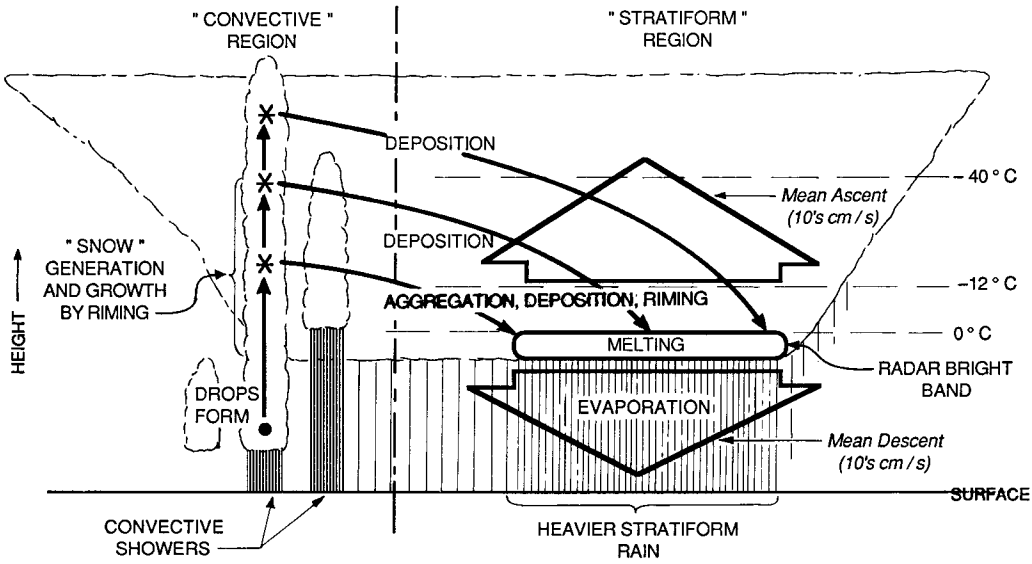

Figure 2. Schematic diagram of the precipitation mechanisms in a tropical cloud system. Solid arrows indicate particle trajectories (adapted from Houze 1989).

(*b*) *Diabatic heating associated with the idealized cloud system*

Houze (1982) considered an arbitrary large-scale region surrounding the idealized MCS (region A in Fig. 1). He then asked, what is the vertical distribution of heating due to the MCS that is felt by the large-scale region? According to his development, this heating H (J/s) is given by

$$H \simeq \underset{\text{(i)}}{\sigma_{\text{cloud}} Q_{\text{rc}}} + \underset{\text{(ii)}}{\sigma_{\text{c}} L_{\text{v}} (c_{\text{cu}} - e_{\text{cd}})} + \underset{\text{(iii)}}{\sigma_{\text{s}} L_{\text{v}} (c_{\text{mu}} - e_{\text{md}})} - \underset{\text{(iv)}}{\sigma_{\text{s}} L_{\text{f}} m} - \underset{\text{(v)}}{\frac{\partial}{\partial p} \sum_i \sigma_i \omega_i (s_i - s_{\text{e}})} \quad (1)$$

where σ_{cloud} is the fraction of A covered by cloud, Q_{rc} is the net radiative heating in cloud, σ_{c} is the fraction of A covered by the convective precipitation region, σ_{s} is the fraction of A covered by the stratiform precipitation area, L_{v} and L_{f} are the latent heats of vaporization and fusion, respectively, c_{cu} is the condensation in convective updraughts, e_{cd} is the evaporation in convective downdraughts, c_{mu} is the condensation in this mesoscale updraught of the stratiform region, e_{md} is the evaporation in the mesoscale downdraught of the stratiform region, m is the melting in the stratiform region (concentrated in a 0·5–1·0 km layer just below the 0 °C level), p is pressure, ω is dp/dt, t is time, s is dry static energy and the subscript i refers to the various subdivisions of the cloud area. Each of the terms in this equation was examined by Houze (1982) for the idealized cloud system. The dominant terms are (ii) and (iii), which are in turn approximately proportional to the mean profiles of vertical velocity $w(z)$ in the convective and stratiform regions, respectively. The vertical profile of w in the convective region, which was dominated by the convective updraughts, was based by Houze on a simple one-dimensional entraining jet model. The magnitude was scaled according to the total precipitation assumed to be falling from the convective region. In the stratiform region, the vertical velocity was assumed to be zero at the melting level (cloud base), near the tropopause (cloud top), and at the earth's surface. Parabolic profiles were assumed to apply both above the melting level, where $w > 0$, and below, where $w < 0$. The magnitudes of w were scaled by the amount of stratiform rain, and assumptions were made

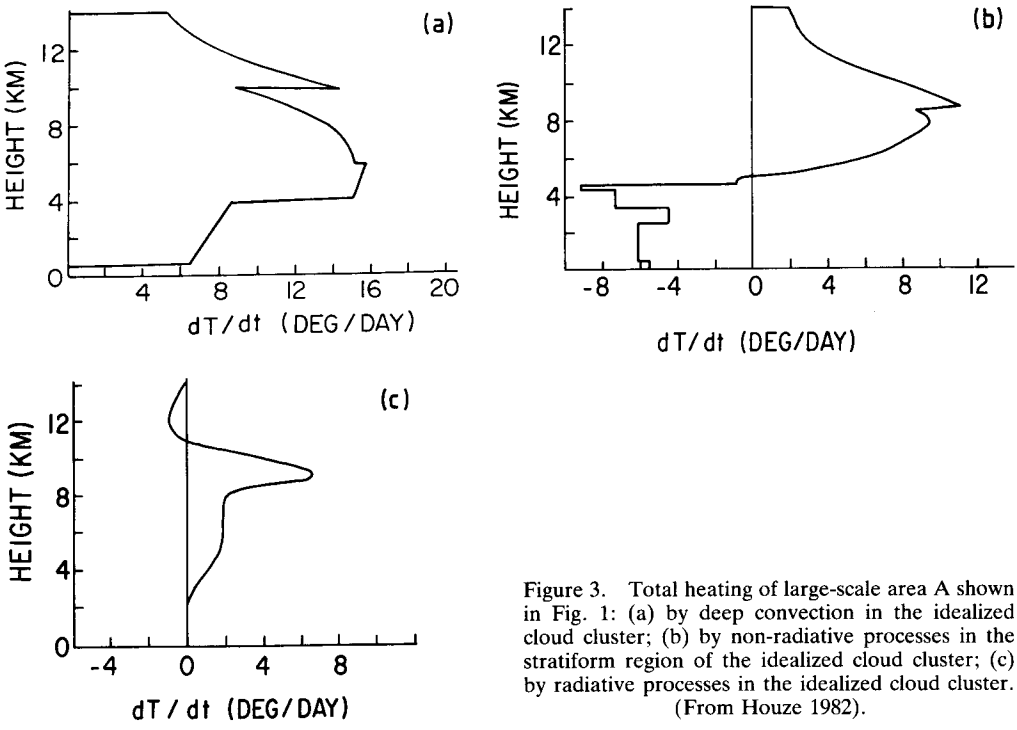

Figure 3. Total heating of large-scale area A shown in Fig. 1: (a) by deep convection in the idealized cloud cluster; (b) by non-radiative processes in the stratiform region of the idealized cloud cluster; (c) by radiative processes in the idealized cloud cluster. (From Houze 1982).

about the water budget of the cloud system. Although there was some evidence to support the vertical profiles assumed in these calculations at the time of Houze's study, there was little observational information to indicate what these profiles really are in MCSs.

Houze's (1982) estimates of the components of the vertical distributions of heating of the large-scale region by the idealized MCS are shown in Fig. 3. The heating by the convective cells is shown in Fig. 3(a). It is dominated by condensation in convective updraughts (c_{cu} part of term (ii) in Eq. (1)) and positive heating extends through the whole troposphere. The individual contributions of convective updraught condensation, downdraught evaporation (e_{cd} part of term (ii) in (1)) and eddy flux convergence of sensible heat (convective updraught and downdraught contributions to term (v) in (1)) are indicated in Fig. 4. In the stratiform region (Fig. 3(b)) updraught condensation (c_{mu} part of term (iii) in (1)) warms the upper troposphere; however, melting and downdraught

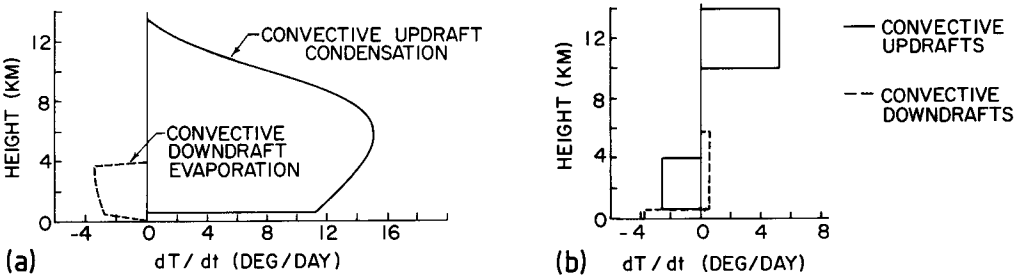

Figure 4. Contributions to the idealized cloud cluster's net convective heating (shown in Fig. 3) by: (a) condensation and evaporation in convective updraughts and downdraughts; and (b) convergence of sensible heat flux by the updraughts and downdraughts in the convective towers. (From Houze 1982).

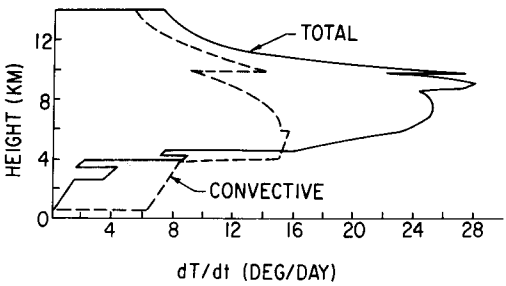

Figure 5. Total heating of large-scale area A shown in Fig. 1 by the idealized cloud cluster (solid curve). The total heating by the convective towers alone (dashed curve, from Fig. 3(a)) is shown for comparison. (From Houze 1982).

evaporation (term (iv) and e_{md} part of term (iii) in (1)) dominate and produce cooling in the lower troposphere. Radiation heating, estimated for daytime conditions from Webster and Stephens's (1980) calculations, is maximum in the upper troposphere (Fig. 3(c)).

The total heating of the large-scale region A by the idealized MCS is obtained by summation of the solid curves in Figs. 3(a, b and c). The result is the solid curve in Fig. 5. This curve gives the sum of the terms on the right-hand side of (1), after the terms have been divided by c_p to give units of °C/d. The heating associated with the convective towers alone (from Fig. 3(a)) is shown for comparison by the dashed curve in Fig. 5.

Since the heating profiles in Figs. 3(a, b and c) are all positive above 5 km, the profiles reinforce each other in the middle to upper troposphere. Consequently, at middle to upper levels, the total heating of the cluster (Fig. 5), including its stratiform and radiative components as well as its convective towers, is much stronger than the heating due to the convective towers alone (compare the solid and dashed curves above 5 km). At lower levels, cooling by evaporation and melting in the stratiform precipitation region of the cluster is significant (negative values below 5 km in Fig. 3(b)). This cooling tends to cancel the heating by convective towers and the total heating at lower levels in the cluster is, therefore, less than that associated with the convective towers alone (i.e. the solid curve lies to the left of the dashed curve below 5 km in Fig. 5).

Johnson and Young (1983) independently verified the heating rates estimated for the stratiform region by Houze (1982) by calculating the heat and moisture budgets of regions containing stratiform regions of tropical MCSs from rawinsonde data obtained during Winter MONEX. From these budgets they diagnosed heating rates that agree very closely with the rates estimated by Houze for the stratiform region of the idealized cloud system (see comparison in Fig. 6). Johnson (1984) then used this result to re-examine the total diabatic heating profile computed by Yanai *et al.* (1973) for a region in the equatorial western Pacific. Assuming that the precipitation in the region was 20% stratiform, he found that Yanai and collaborators' heating profile, which has a peak near 450 mb (6 km), is the consequence of two distinctly different circulation features: (i) the mesoscale stratiform region, which has a heating peak near 350 mb (8 km) and a cooling peak near 700 mb (3 km), and (ii) the cumulus, which produces a heating peak centred near 600 mb (4 km) (see Fig. 7).

Johnson's (1984) diagnosed convective region heating profile in Fig. 7 has a lower-level maximum than suggested by Houze's (1982) profile for the region of convection. Johnson suggests that heat flux divergence associated with small non-precipitating cumulus at lower altitudes might be partially responsible for the difference, since the effects of small cumulus are included in his estimate, but not in Houze's calculations. However, the reason for this difference may lie in Houze's choice of a one-dimensional weakly

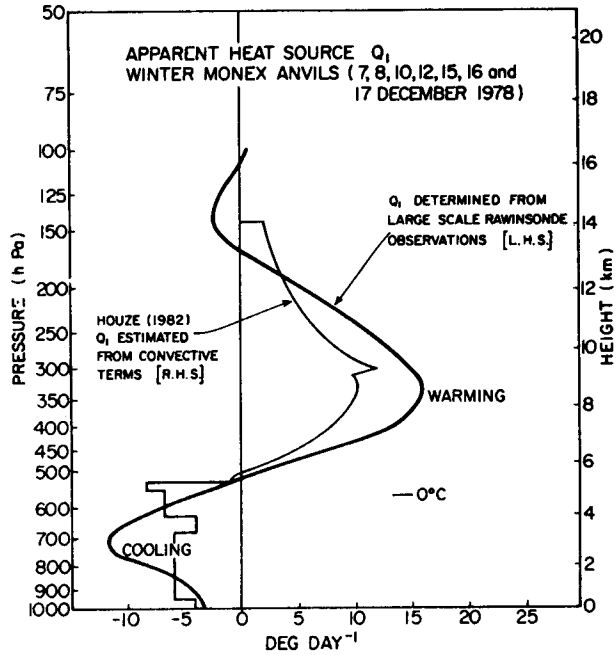

Figure 6. Comparison of apparent heat source Q_1 inferred from Winter MONEX rawinsonde data by Johnson and Young (1983) for regions containing stratiform regions of cloud clusters (heavy curve) with that obtained by Houze (1982) using observations of cloud structure and precipitation (light curve). Left-hand side (right-hand side) refers to left-hand side (right-hand side) of Johnson and Young's Eq. (1). The curve from Houze (1982) represents the total heating by non-radiative mesoscale processes. From Johnson and Young (1983).

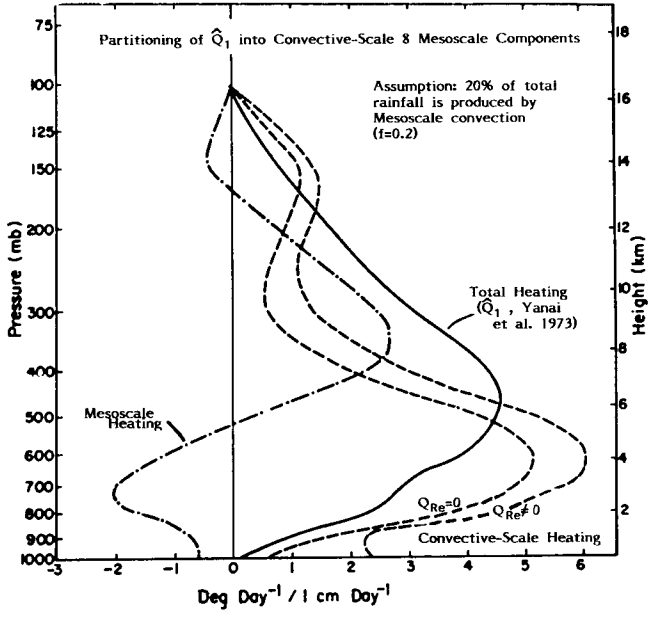

Figure 7. Partitioning of the normalized apparent heat source Q_1 into convective-scale (cumulus) and mesoscale components for $f = 0{\cdot}2$; f is the fraction of the total rainfall assumed to be produced by mesoscale stratiform anvils. Curve marked Q_{Re} refers to radiative heating profile in the environment of the convective clouds. From Johnson (1984).

entraining jet to represent the cells producing the rain in the idealized MCS. Such a jet may be characterized by too much mass flux and hence too much heating at upper levels (further discussion in section 4(*c*)(ii).

In a further examination of the rawinsonde data in the vicinity of Winter MONEX MCSs, Johnson (1986) has found that while the apparent heat source in the lower troposphere beneath the stratiform cloud systems is negative owing to hydrometeor melting and evaporating, the time tendency of temperature is actually positive. This low-level warming is attributed to unsaturated descent in the mesoscale downdraught occupying the lower troposphere in the stratiform region.

3. Applicability of the conceptual model

(*a*) *Tropical cloud clusters*

Houze's (1982) conceptual model (Fig. 1) was originally designed to resemble near-equatorial MCSs, which are traditionally referred to as tropical 'cloud clusters'. The rainfall in most regions within 15° latitude of the equator is dominated by cloud clusters. In such regions, which include those investigated intensively during GATE (Houze and Betts 1981) and Winter MONEX (Johnson and Houze 1987), it is the largest cloud clusters that are responsible for the bulk of the rain.

Williams and Houze (1987) traced the life histories of all the cloud clusters in Winter MONEX and found that most of the cumulative cloud cover colder than −60 °C (indicated by satellite data) was accounted for by a few clusters that reached extremely large size. About 85% of the cumulative cloud cover was associated with clusters that had a maximum size of 3×10^4km^2 or more (Fig. 8). To the extent that the area of cold cloud top is correlated with the amount of the area covered by rain, this result strongly suggests

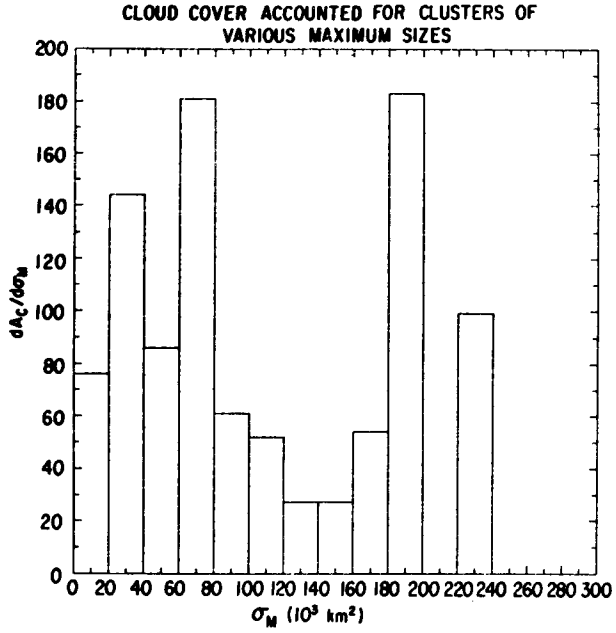

Figure 8. Areal cloud cover accounted for by Winter MONEX cloud clusters of various maximum sizes. σ_M is the maximum size attained by a cluster in its lifetime; $(dA_c/d\sigma_M)d\sigma_M$ is the total area covered by all clusters that had maximum sizes in a size range of width $d\sigma_M$. From Williams and Houze (1987).

that a very high percentage of the rainfall in the region came from the few very largest clusters. Therefore, in considering diabatic heating effects, the large clusters are of paramount importance.

The area covered by rain in a large cloud cluster is broken up into numerous discrete rain areas. However, the total (cumulative) rain area within the cluster is usually dominated by one or only a few very large mesoscale precipitation areas. In GATE, 72% of the area covered by radar echo was accounted for by rain areas $> 10^3 km^2$ and within these large rain areas were found several (2–10) intense convective-scale showers (Houze and Betts 1981). Much of the remainder of the area covered by these big rain areas consisted of stratiform echo, typically characterized by a radar bright-band signature at the melting level (Leary and Houze 1979b). A similar cloud cluster radar echo structure was observed in Winter MONEX (Houze *et al.* 1981).

Studies of radar data obtained in GATE and Winter MONEX, as well as in the more recent field programmes, COPT '81 (Convection Profonde Tropicale 1981) and EMEX (Equatorial Mesoscale Experiment), reveal several types of horizontal patterns in which the convective and stratiform precipitation are arranged within the rain areas of large cloud clusters.

The type of cloud cluster that has been studied most extensively is the propagating squall line, in which the convective cells are arranged in an arc-shaped line trailed by the stratiform precipitation region (e.g. Fig. 9). The precipitation structures of these MCSs have been documented over the equatorial Pacific (Zipser 1969), the equatorial Atlantic (Houze 1977; Zipser 1977; Gamache and Houze 1982, 1983, 1985; Houze and Rappaport 1984; Wei and Houze 1987) and the equatorial land masses of West Africa (Hamilton and Archbold 1945; Sommeria and Testud 1984; Roux 1987; Chong *et al.* 1987) and North Australia (Drosdowsky 1984).

The well defined structure and motion of the propagating squall lines make them amenable to study, and it is probably for this reason that they have been given the most

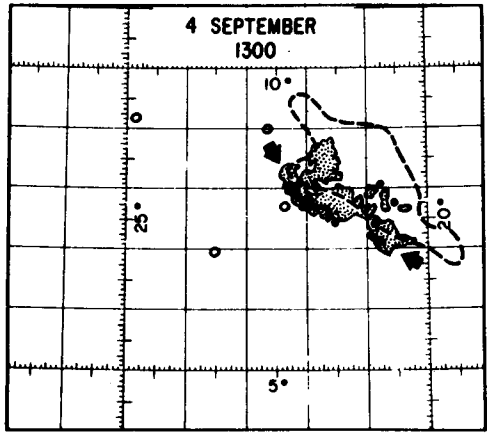

Figure 9. Cloud and precipitation pattern associated with GATE squall-line system of 4 September 1974. Dotted region encloses low-level precipitation detected by radar. Black indicates regions of precipitation intensity in excess of 38 dBZ. Dashed line is satellite infrared isotherm for −47 °C, which corresponds to the intersection of the upper-level cloud shield with the 11 km level. Arrows locate end points of squall line. From Houze (1977).

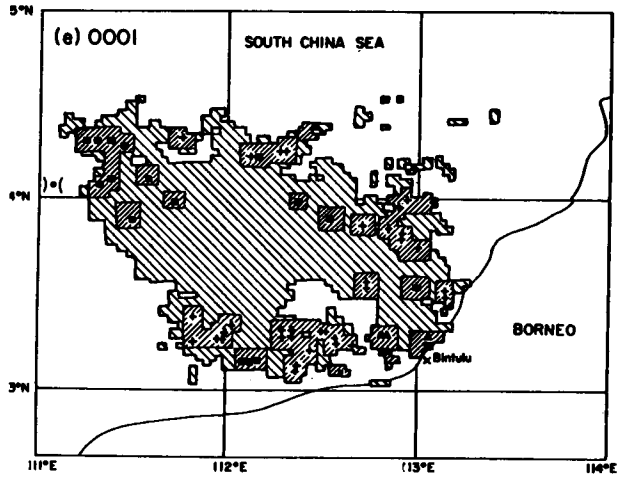

Figure 10. Radar-echo patterns at 3 km altitude in a Winter MONEX cloud cluster at 0001 GMT 10 December 1978. The radar was located at Bintulu (3·2°N 113·1E). The thin curve shows the northern coast of Borneo. Light shading is stratiform precipitation, heavy shading is convective. The dBZ values of objectively identified convective cores are indicated by dots (1–20 dBZ), crosses (21–30 dBZ), squares (31–40) dBZ and triangles (>40 dBZ). From Churchill and Houze (1984).

attention in the literature. Several other types of convective–stratiform organization have, however, also been documented in tropical cloud clusters. Sometimes the rain patterns in cloud clusters exhibit leading line, trailing stratiform structure but with convective lines that are more slowly moving, less arc-shaped, less continuous or otherwise less well defined (Leary and Houze 1979a; Warner *et al.* 1980; Barnes and Sieckman 1984; LeMone *et al.* 1984). In other cases, the rain patterns are related to surface features. For example, in Winter MONEX, convective regions were forced by local convergence associated with coastlines in the Malaysian–Indonesian complex of islands and peninsulas; nonetheless, large stratiform regions developed in association with the convection, and vertical cross-sections through the precipitation areas were rather similar to those through squall lines with trailing stratiform regions (Houze *et al.* 1981). In a Winter MONEX case examined by Churchill and Houze (1984), a large stratiform region was surrounded by convective cells (Fig. 10); the convective cells to the south-east were associated with coastal convergence and relatively stationary, while the convection located to the north-west propagated farther out to sea like a poorly organized squall line.

In EMEX, cloud clusters were observed by aircraft radar over the tropical ocean north of Australia. The precipitation in these clusters was sometimes organized with convective lines parallel to the low- to mid-level monsoon flow, with stratiform rain occurring on both sides of the line (Fig. 11(a)). In other cases, the rain was organized into the squall-line mode with arc-shaped leading convective line and trailing stratiform precipitation (Fig. 11(b)). Sometimes, as in the case of Fig. 11, the flow-parallel lines evolved into squall lines. In still other cases in EMEX, the convective cells occurred in an area rather than a line. The airborne radar data showed that the stratiform areas in these clusters tended to form where cells dissipated. For example, the maximum of stratiform rain in the vicinity of the aircraft flight track in Fig. 11(b) was previously the location of active convective cells.

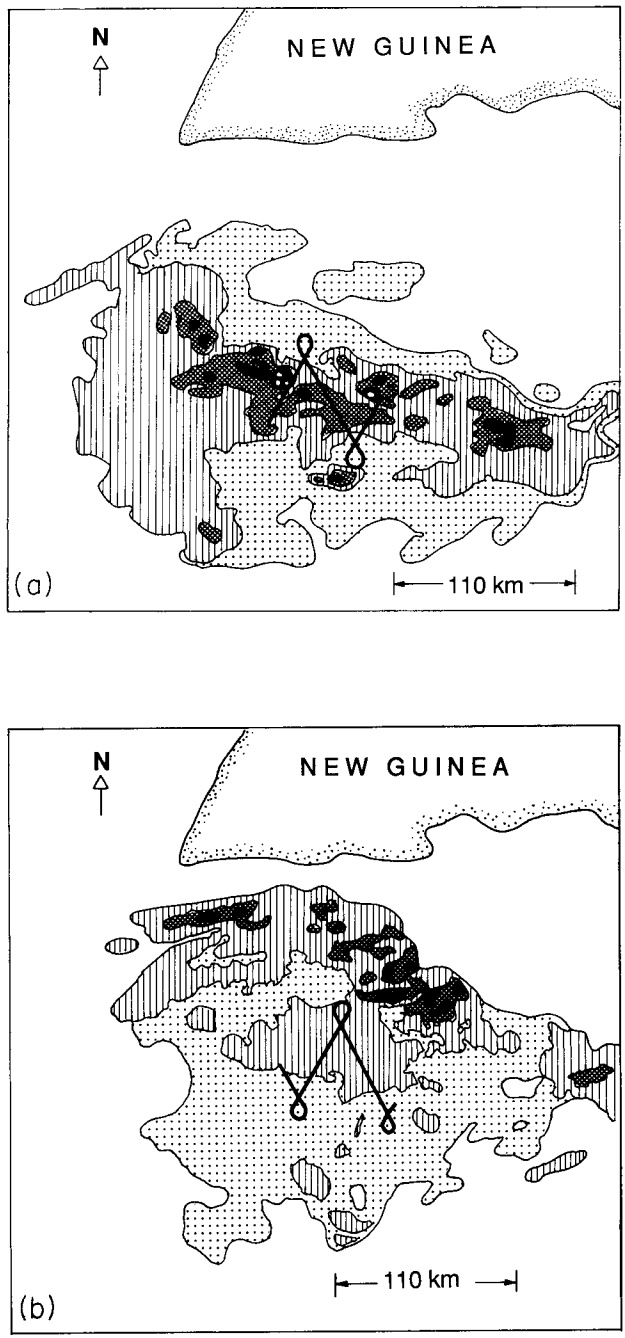

Figure 11. Radar echo patterns in a cloud cluster observed during EMEX. Data were collected with a C-band radar aboard a National Oceanic and Atmospheric Administration WP3D aircraft. Composite echo patterns were observed during (a) 2112–2142 and (b) 2314–2344 GMT 2 February 1987. Shading levels are for intensity thresholds of 1 (approximately), 20, 25, 30 and 35 dBZ. Heavy lines show flight track for the period of data collection.

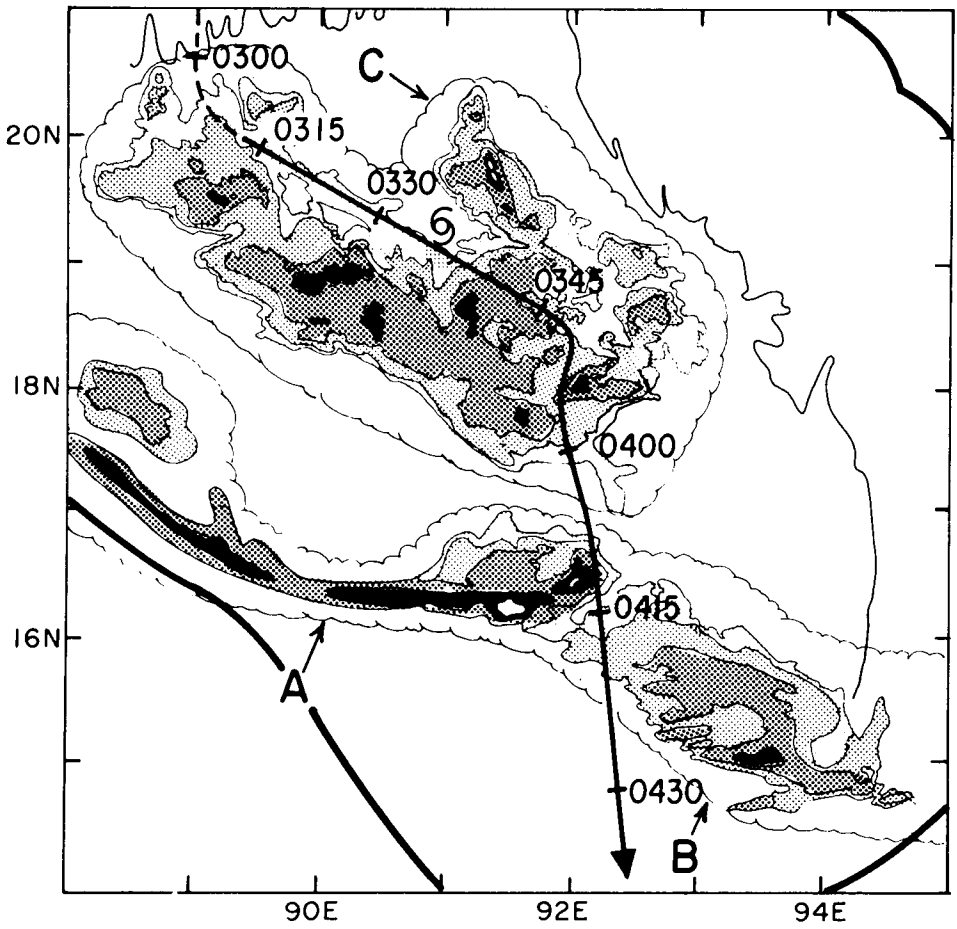

Figure 12. Aircraft data obtained in a depression over the Bay of Bengal on 5 July 1979. Radar observations are shown by shading thresholds of 1, 20, 30 and 35 dBZ. Flight track of the P3 is indicated by the dashed and solid lines. The solid line indicates that portion of the flight where radar data were collected, and from which the composite was generated. Dashed lines show portions of the flight track where radar data were not being collected. Numbers indicate times (UTC) every 15 min at the corresponding hash marks on the flight track. The heavy, bold curve outlines the area over which radar data were obtained. The scalloped line indicates approximate cloud boundaries, based on satellite imagery and microphysical observations. Thin solid line is coastline. From Houze and Churchill (1987).

(*b*) *Bay of Bengal depressions*

A considerable amount of monsoon rain occurs outside of near-equatorial regions and is controlled by processes not found at those lower latitudes. For example, much of the rainfall of northern India, which lies in the subtropics, is associated with Bay of Bengal depressions (Ramage 1971; Rao 1976; Godbole 1977). During Summer MONEX, the precipitation pattern in one long-lived Bay of Bengal depression was documented extensively by aircraft (Sanders 1984; Warner 1984; Warner and Grumm 1984; Houze and Churchill 1987). Houze and Churchill's analysis of the airborne radar and cloud physics data shows that the precipitation in the disturbance occurred in rather elongated mesoscale rain areas 100–300 km in horizontal dimension (e.g. Fig. 12). These mesoscale precipitation features resembled the rain areas of the near-equatorial cloud clusters

described in section 3(*a*). Each mesoscale precipitation feature contained intense convective cells, but overall most of the area covered by rain was stratiform. The convective cells in the mesoscale features were sometimes arranged in rapidly moving arc-shaped lines (feature A in Fig. 12), while in other cases the convective cells were more randomly embedded in the stratiform rain (features B and C in Fig. 12).

Houze and Churchill further found that the particle growth mechanisms indicated by the cloud microphysical data collected aboard the aircraft passing through the precipitation areas in the Bay of Bengal depression were consistent with the conceptual model in Fig. 2. Above the melting level, mesoscale updraught motion in stratiform regions was apparently strong enough to support growth of ice particles by vapour deposition, but not strong enough to prevent general sedimentation of the particles, which were drifting down to the melting level.

(*c*) *Mid-latitude mesoscale convective systems*

Some early studies indicated that lines of deep mid-latitude convection are at times trailed by broad areas of light rain from stratiform cloud (Newton 1950; Fujita 1955; Pedgley 1962). Newton and Fankhauser (1964) pointed out that when portions of convective lines weaken, the result is a stratiform precipitation area.

Despite these studies, the possible importance of the stratiform precipitation areas associated with mid-latitude convection has only recently begun to receive emphasis. Ogura and Liou (1980) recognized the close similarity of an Oklahoma squall line to tropical squall lines with trailing stratiform regions. Maddox (1980) identified the mid-latitude 'mesoscale convective complex (MCC)' as a long-lived oval-shaped satellite-observed cloud shield with extremely low cloud top temperature. Fritsch *et al.* (1986) found that MCCs account for about 50–60% of the warm season rainfall over the central United States, and Maddox (1980) described how these complexes developed regions of stratiform rain during their mature stages. Smull and Houze (1985) found that the squall line system studied by Ogura and Liou had the cloud top characteristics (temperature, size, shape and duration) of a Maddox MCC. However, the leading-line, trailing-stratiform structure observed in that case, though common, is not typical of all MCCs. As in tropical cloud clusters, stratiform rain in mid-latitude mesoscale convective systems appears in a variety of horizontal patterns, of which the leading-line, trailing-stratiform configuration is one type. Figure 13 shows some examples of precipitation patterns in mid-latitude MCSs observed in the Oklahoma–Kansas PRE-STORM (Preliminary Regional Experiment for the Stormscale Operational and Research Meteorology Program—Central Phase) field programme. A squall line with trailing stratiform precipitation is shown in Fig. 13(a). It exhibits a well defined example of the secondary maximum of precipitation seen in the stratiform region (centred north–west of the Wichita (ICT) radar site). This area of heavier stratiform rain was illustrated in the conceptual model of MCS precipitation mechanisms in Fig. 2, where it was related to the fallout of ice particles from the convective line. A squall line with stratiform precipitation located preferentially to the north–west of the line is shown in Fig. 13(b). This arrangement of the precipitation is related to a mid-level mesoscale vortex in the stratiform region.

(*d*) *Hurricanes*

In some parts of the tropics, about 25% of the precipitation is produced by tropical cyclones (Simpson and Simpson 1966). The structure and kinematics of precipitation in tropical cyclones bear some resemblance to that in the other types of mesoscale systems considered in this paper. Vertical cross-sections across the inner-core region of a hurricane typically show stratiform precipitation in an annular region just outside the convective

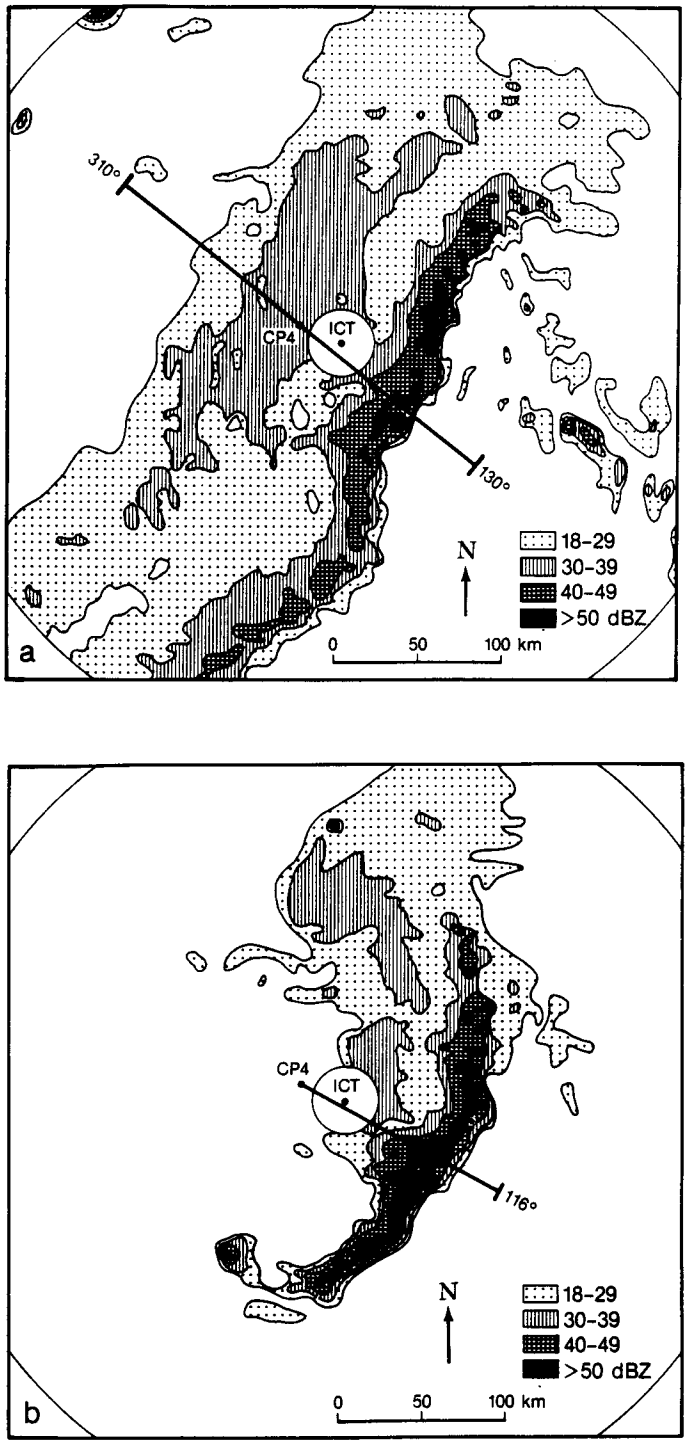

Figure 13. Low-level (0·7° elevation) reflectivity structure from Wichita, Kansas (ICT) WSR-57 S-band radar from Smull and Houze (1987). Positions of CP3 and CP4 C-band Doppler radars are indicated. Superimposed straight line indicates azimuth angles of vertical cross-sections shown by Smull and Houze but not shown here. Ground clutter region within 20 km of ICT has been blanked out. Horizontal scale and north direction are indicated. (a) Reflectivity pattern for 2140 CST 10 June 1985. (b) Reflectivity pattern for 0701 CST 28 May 1985.

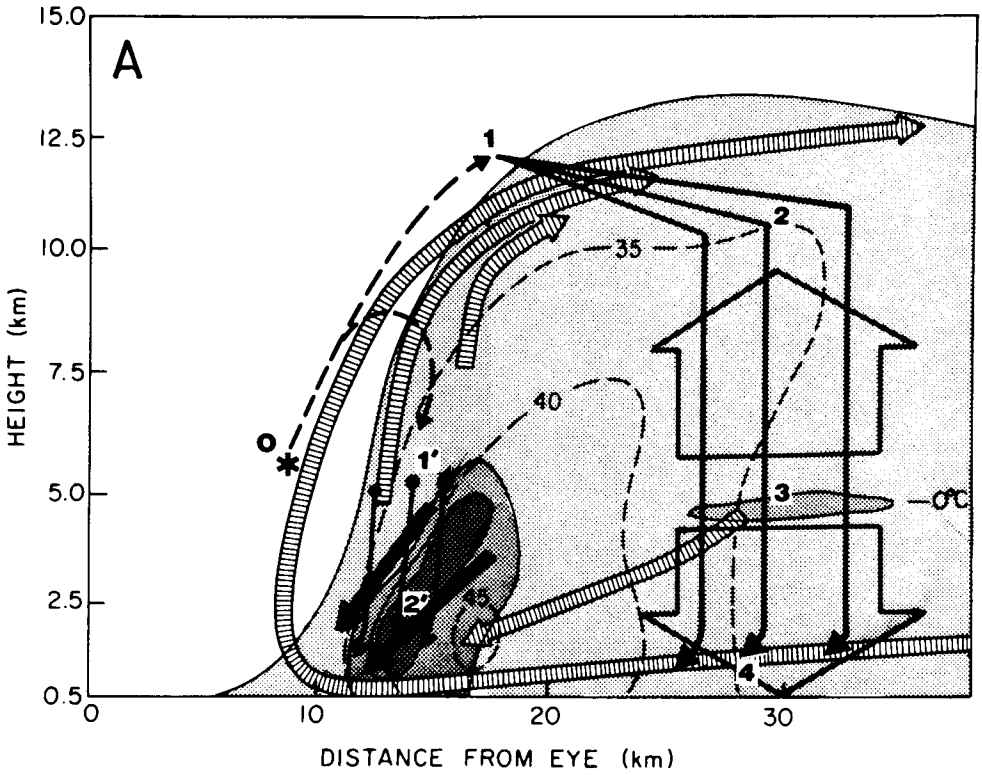

Figure 14. Schematic of the radius–height circulation of the inner core of hurricane Alicia. Shading depicts the reflectivity field (5, 30 and 35 dBZ). The primary circulation (V_θ m s^{-1}) is depicted by dashed lines and the secondary circulation by the wide hatched streamlines. Convective downdraughts are denoted by the thick solid arrows. Mesoscale up- and downdraughts are shown by the broad arrows. The level of the 0 °C isotherm is labelled. Hydrometeor trajectories are denoted by dashed and solid lines labelled 0–1–2–3–4 and 0–1′–2′. Horizontal projections of these trajectories are shown in Fig. 15. From Marks and Houze (1987).

eyewall (see Fig. 14, from Marks and Houze (1987)). Radial outflow aloft carries ice particles outward from the eyewall. These particles fall slowly through a region of general weak ascent, as in the schematic model in Fig. 2. As they fall, they are swirled up to 1½ times around the storm by the vortex winds before they reach the melting level (Fig. 15, also from Marks and Houze (1987)).

In addition to occurring in the inner-core region, convective–stratiform structure is also sometimes seen in the outer extremities of the storm, where convective cells can be located on the upwind end of a spiral band, while ice particles detrained from the cells are carried downwind into a stratiform region of the band (Atlas *et al.* 1963).

(*e*) *Summary of applicability of the conceptual model*

From subsections 3(*a–d*), it is evident that the conceptual model designed initially to describe tropical cloud clusters applies to a wide variety of MCSs, including various types of tropical cloud clusters, mid-latitude convective complexes, subtropical monsoon depressions and hurricanes. In all of these precipitation systems, large areas of stratiform rain accompany deep convection. The different types of systems vary in the horizontal arrangement of the convective and stratiform precipitation. However, in vertical cross-section they all resemble Figs. 1 and 2.

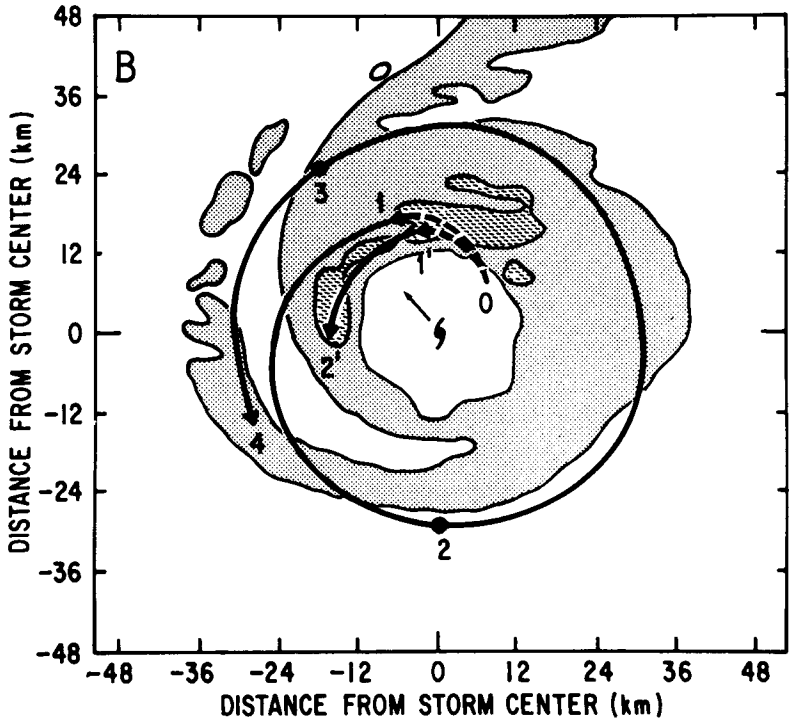

Figure 15. Plan view of the low-level reflectivity field in the inner core of hurricane Alicia. Superimposed horizontal projections of calculated trajectories of precipitation particles falling from 12 to 1 km altitude correspond to those shown in Fig. 14. Reflectivity contours are for 20 and 35 dBZ. Storm centre and direction of motion are also shown. From Marks and Houze (1987).

4. Observed vertical velocity profiles in convective and stratiform regions

In this section, we examine observational evidence regarding the vertical distribution of vertical air motion in the convective and stratiform regions of MCSs. These results, which have been obtained mostly within the last five years, can be used to indicate whether the vertical profiles of diabatic heating suggested by Houze (1982) to apply within the convective and stratiform regions of his idealized MCS (section 2(*b*)) are in fact reasonable.

(*a*) *Stratiform region profiles*

Since 1982, the vertical profile of w in the stratiform regions of MCSs has been determined by four different methods: composite analysis of rawinsonde and aircraft-observed winds, single-Doppler weather radar[1] analysis, synthesis of dual-Doppler weather radar observations and analysis of vertical-incidence wind profiler[2] measurements. These profiles have, moreover, been determined for MCSs in various

[1] Weather radar refers to a 5- or 10-cm wavelength radar (15–30 GHz), which primarily detects precipitation targets.

[2] Wind profiler refers to a class of meteorological radar in the VHF to UHF frequency range (30–300 MHz) that is designed to detect atmospheric targets consisting of air density fluctuations and may be operated in clear or cloudy conditions.

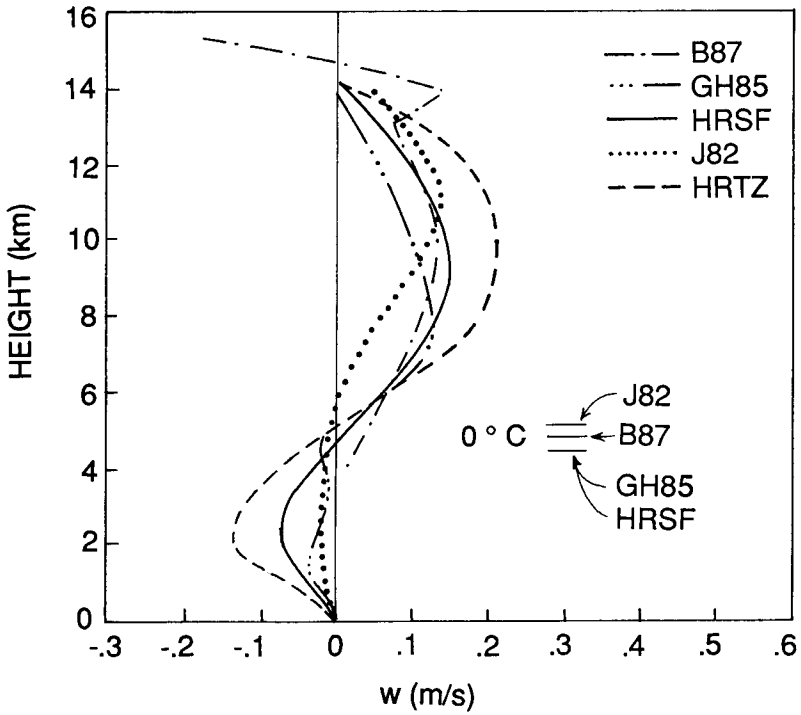

Figure 16. Tropical oceanic and island stratiform-region vertical velocity profiles. The GH85 curve is from Gamache and Houze's (1985) composite sounding and aircraft wind analysis of the 12 September 1974 GATE squall line. The HR curves are from Houze and Rappaport's (1984) composite sounding and aircraft wind analysis of the 28 June 1974 GATE squall line; HRTZ is for the transition zone and HRSF is for the stratiform region proper. Curve J82 is from Johnson's (1982) rawinsonde analysis of Winter MONEX cloud clusters. The B87 curve is from the study of Balsley *et al.* (1988); it shows the two-year average vertical velocity during periods of light rain (0·5–12·7 mm/h) at Pohnpei in the tropical western Pacific.

meteorological settings: oceanic tropical, tropical island, continental tropical and mid-latitude continental. These results are summarized in Figs. 16–18.

(i) *Tropical oceanic and island cases.* The tropical oceanic and island cases (Fig. 16) all show upward motion in the upper troposphere. The Johnson (1982) curve (J82) was obtained from his composite analysis of ship rawinsonde data in the vicinity of stratiform regions of Winter MONEX cloud clusters over the South China Sea. The Houze and Rappaport (1984) and Gamache and Houze (1985) curves (HRTZ, HRSF and GH85) were determined from composite analyses of ship rawinsondes and aircraft data taken in and near GATE squall line systems in the eastern tropical Atlantic. The Balsley *et al.* (1988) curve (B87) was obtained by averaging vertical-incidence profiler data from a single island station in the west Pacific (Pohnpei) for all of the light rain situations (0·5–12·7 mm/h) in a two-year period. These estimates all agree well, indicating a maximum value of about 15 cm/s in the upper troposphere (7–11 km). The curves approach zero between 4 and 6 km height and indicate downward motion below this level. The curves derived from sounding data were constrained by mass balance assumptions to go to zero at the tropopause level. The profiler curves were subject to no such boundary condition and indicate that rather strong descent was occurring in the lower stratosphere, just above the stratiform cloud layer (above ≈15 km in Fig. 16). This descent remains to be explained but may be associated with the strong divergent horizontal outflow that characteristically occurs at the tops of MCSs (Ninomiya 1971a, b; Maddox 1980, 1981;

Fritsch and Maddox 1981a, b; Maddox *et al.* 1981). This divergence may be partially compensated by subsidence in the lower stratosphere.

(ii) *Continental tropical case.* The continental tropical case (Fig. 17) was a squall system over western equatorial Africa during COPT '81 on 22 June 1981. The vertical velocity was determined by Chong *et al.* (1987) from single-Doppler radar by the Velocity Azimuth Display (VAD) analysis method in which w is computed from the radial wind component measured around the edge of a cylindrical volume centred on the radar site (Browning and Wexler 1968; Srivastava *et al.* 1986). Chong *et al.* computed the vertical velocity profiles in the stratiform region at successive distances from the leading convective squall line. Figure 17 shows the profiles at three positions; profiles 2, 3 and 4 were taken at 80, 120 and 150 km to the rear of the squall line, respectively. All three profiles show more intense upward velocities in the upper troposphere (25–45 cm/s peak values) than do the oceanic tropical profiles in Fig. 16. The lower troposphere is characterized by stronger descent than the oceanic cases. The level of zero vertical velocity was near the 0 °C level in profiles 3 and 4, but about 2 km higher in profile 2.

It is not certain whether the greater magnitudes of w seen in Fig. 17 compared with Fig. 16 are meteorological differences between land and ocean convection, or whether they are the result of the different observational and analysis techniques. The oceanic results determined by composite analysis (Johnson 1982; Houze and Rappaport 1984; Gamache and Houze 1985) represent averages of smoothed data over large areas, while those determined from profiler data (Balsely *et al.* 1988) were averaged over many cases. The continental tropical case in Fig. 17 was obtained from high resolution single-Doppler radar at specific points and times within a well defined mature storm system.

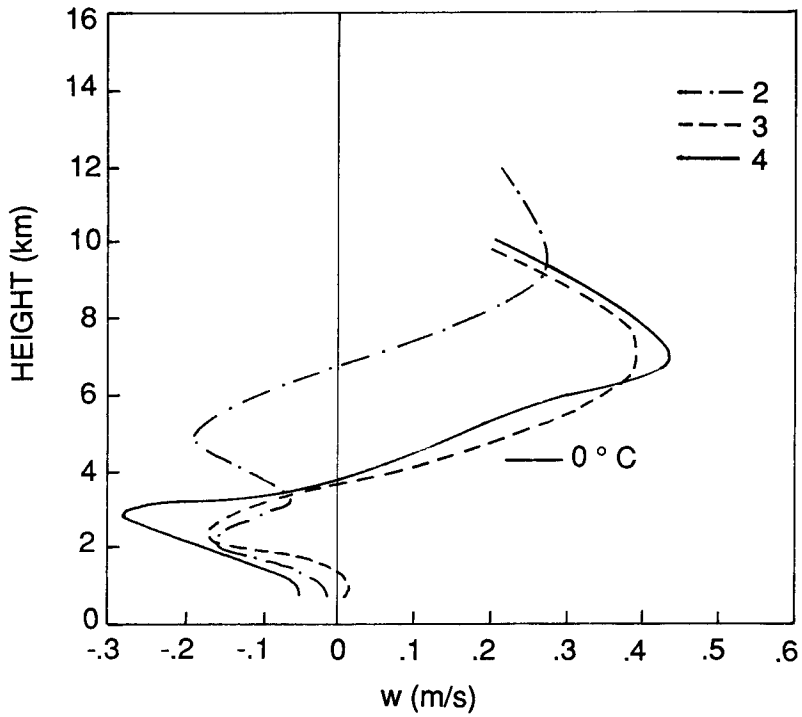

Figure 17. Stratiform-region vertical velocity profiles for the continental tropical squall-line system over Ivory Coast in western Africa, 22 June 1981. Profiles were derived by single-Doppler radar analysis by Chong *et al.* (1987). Curves are shown for three locations in the stratiform region; numbering system corresponds to Chong *et al.* (1987).

(iii) *Mid-latitude continental cases.* The mid–latitude case illustrated in Fig. 18(a) was examined by two methods. The OL profile was derived by Johnson (1982) from Ogura and Liou's (1980) rawinsonde composite analysis of a squall-line system over Oklahoma. Johnson averaged Ogura and Liou's results over the 150 km-wide region containing the stratiform precipitation. The two curves labelled SH1 and SH2 were obtained by Smull and Houze (1987) by synthesis of wind observations by two Doppler radars for two subregions of the same stratiform region at a specific time in the storm's lifetime. Curve SH1 is for a 20 km-wide subregion immediately behind the convective line, while curve SH2 is for a subregion of similar width lying immediately behind the first region. The negative w at the top of the profile is an artifact of the analysis technique, which involved a variational adjustment, and a relatively small amount of data at these levels.

When curves SH1 and SH2 are compared to the averaged Ogura–Liou data (curve OL), we see how the effects of compositing and averaging reduce the magnitudes of the maxima and minima of the diagnosed w profiles. Nonetheless, even the averaged sounding composite data in this case exhibits maxima and minima that are about a factor of two greater than those in the tropical oceanic cases examined by similar methodology (cf. curve OL in Fig. 18(a) and the three composite sounding curves in Fig. 16). However, the sounding data in the Oklahoma case were of higher quality and resolution than the oceanic tropical soundings; so even this comparison cannot be regarded as conclusive. Moreover, the GATE squall lines represented by the Houze and Rappaport (1984) and Gamache and Houze (1985) cases were not the most intense (in terms of radar reflectivity observations) seen in GATE. The GATE oceanic squall line described by Houze (1977) had more intense reflectivity (i.e. rainfall rates) and if a composite sounding analysis had been done for that case, stronger ws might have been found.

The dual-Doppler-derived w profiles (curves SH1 and SH2 in Fig. 18(a)) indicate peak upper tropospheric updraught velocities of 40 cm/s and lower tropospheric downdraught magnitudes of 15–40 cm/s. They also indicate that immediately behind the convective line the mesoscale descent layer was deeper and originated about 2 km above the 0 °C level, whereas somewhat farther behind the line the descent was shallower, originating at the 0 °C level. This behaviour resembles that seen in the continental tropical system represented in Fig. 17.

Two more mid-latitude cases have been studied. The case represented in Fig. 18(b) (from Rutledge *et al.* 1988) occurred in Kansas and Oklahoma, while that in Fig. 18(c) (from Srivastava *et al.* 1986) occurred in Illinois. The w profiles for these storms were determined by the single-Doppler VAD technique. Both storms were squall lines with trailing regions of stratiform rain, and their w profiles strongly resemble those of the Oklahoma case in Fig. 18(a) and the continental tropical case in Fig. 17.

The case in Fig. 18(b) exhibited the strongest stratiform ws of any case. The horizontal pattern of radar reflectivity was shown in Fig. 13(a). The maxima of upward motion in the upper troposphere seen in Fig. 18(b) were 50–60 cm/s, while the descent at lower levels reached 45–65 cm/s. Profiles are shown for three locations in the stratiform region. Curves 1 and 2 were located near the northern edge of the stratiform region. The top of the descent layer was 2 km above the 0 °C level in these two curves, while in curve 3, obtained farther south nearer the centre of the stratiform region, the top of the descent layer was at the 0 °C level. In curve 1, the maximum w in the ascent layer was lower (7 km) than in the other two profiles, which were located farther rearward in the stratiform region and exhibited maxima of w at about 11 km. The deeper descent layer on the northern edge of the system is attributed by Rutledge *et al.* (1988) to a deeper layer of dry inflow from the rear of the system at that location. The upward velocity of 10 cm/s near the ground in curve 2 is associated with the mesoscale wake low that characterizes

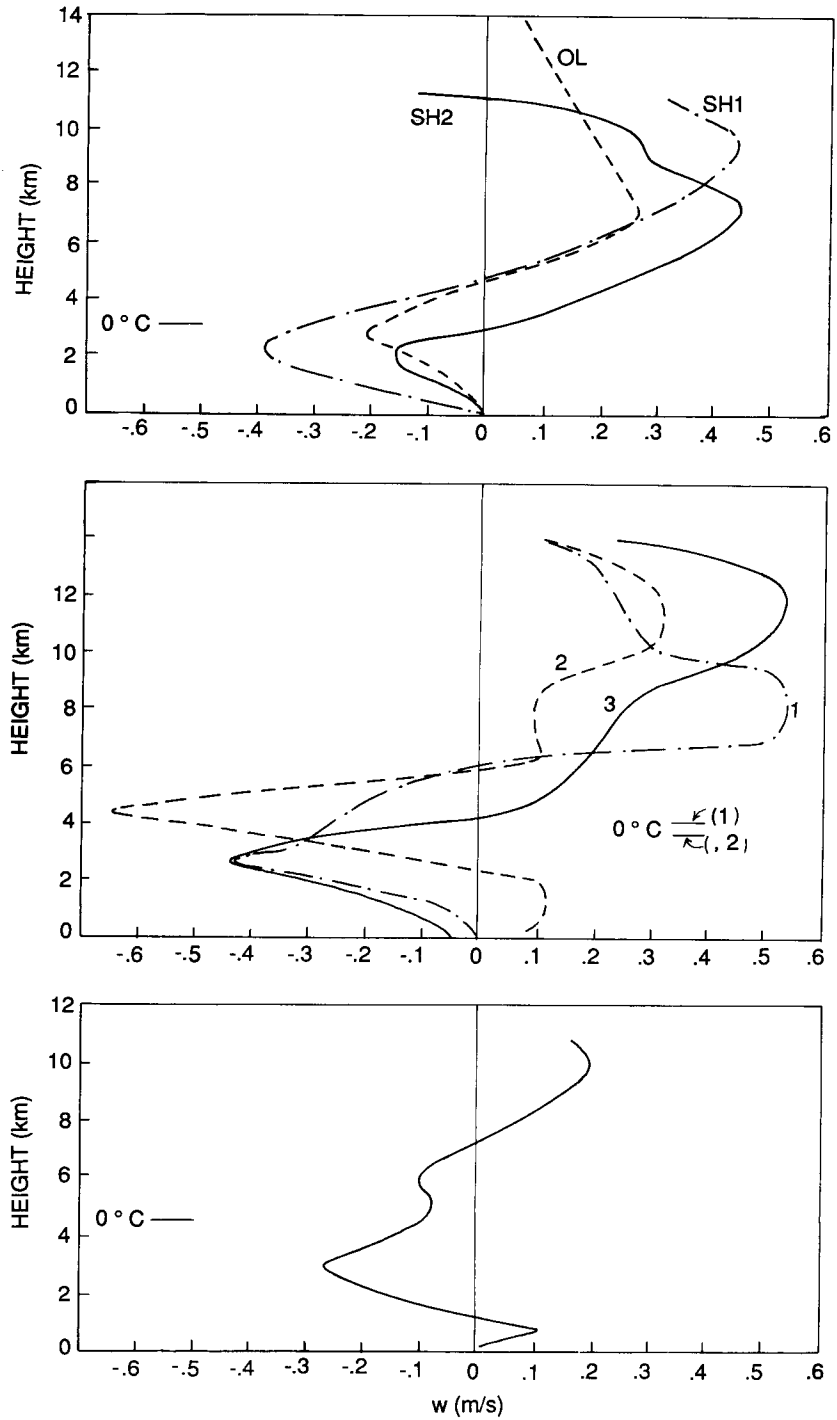

Figure 18. Stratiform-region vertical velocity profiles for three mid-latitude continental squall-line systems. (a) Oklahoma squall line of 22 May 1976. Curve OL is from Ogura and Liou's (1980) composite rawinsonde analysis. The other two curves are from Smull and Houze's (1987) dual-Doppler radar analysis. SH1 is for the transition zone and SH2 is for the stratiform region proper. (b) Kansas squall line of 11 June 1985 (see Fig. 13(a)). Profiles were derived by single-Doppler radar analysis. Curves 1 and 2 are from the CP3 Doppler radar; curve 3 is from the CP4 radar. Locations of CP3 and CP4 radars are shown in Fig. 13(a). (c) Illinois squall line of 17 June 1978. Curve is from single-Doppler analysis of Srivastava *et al.* (1986).

that location (Fujita 1955; Pedgley 1962; Johnson and Nicholls 1983; Johnson 1986; Johnson and Hamilton 1988).

The Illinois case represented in Fig. 18(c) has characteristics similar to the foregoing cases. It is particularly similar to profile 2 in Fig. 18(b), in which the shallow layer of upward velocity is seen near the ground.

(*b*) *Convective region profiles*

Observational studies of the vertical profiles of w in the convective regions of MCSs have been carried out by a variety of methods; however, the results are not as consistent from case to case as for the stratiform regions. One difficulty with the convective regions is the small scale of the individual updraughts and downdraughts and the problems associated with sampling them, either individually or as a group. The following subsections first summarize information available on the structure and intensities of the individual updraughts in MCSs then examine results that diagnose the mean vertical motions in regions of MCSs containing ensembles of draughts.

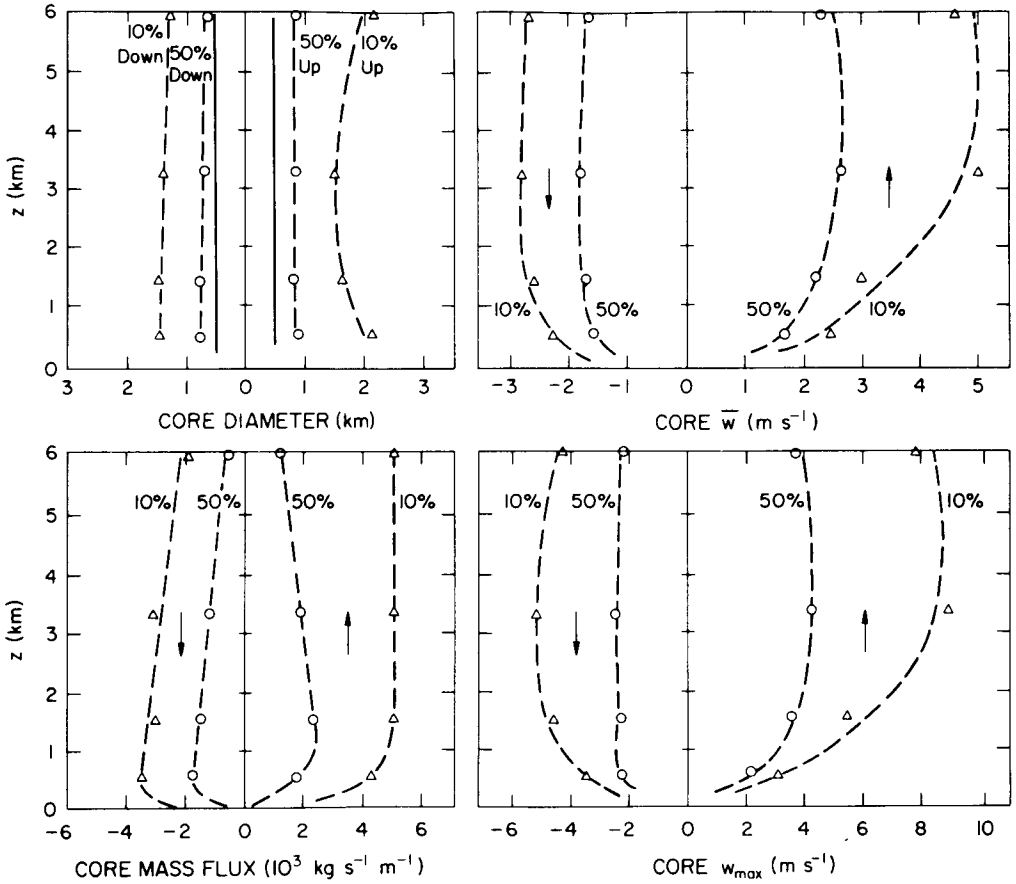

Figure 19. Aircraft-observed properties of convective updraughts and downdraughts in oceanic tropical convection in GATE. Variation with altitude of median (50%) and 10% level (stronger than 90% of the population) updraught and downdraught cores, with respect to core diameter, mean vertical velocity of cores, maximum 1 s vertical velocity within core, and core mass flux. From LeMone and Zipser (1980).

(i) *Individual updraughts and downdraughts.* The scales and intensities of convective updraughts and downdraughts in oceanic tropical MCSs were investigated by LeMone and Zipser (1980). Using GATE aircraft measurements of w, they derived statistics of vertical velocity 'cores', which were defined to exist wherever $w > 1$ m/s continuously over a horizontal flight track segment ≥ 500 m. The diameters and mean and maximum velocities of the cores are indicated as functions of height in Fig. 19. The cores were nearly all <2 km in diameter at all altitudes, and their peak intensities ($|w_{max}|$) tended to be <8 m/s for updraughts and <5 m/s for downdraughts. Zipser and LeMone (1980) compared their results with data from the Thunderstorm Project (Byers and Braham 1949) and found that the GATE updraughts and downdraughts were about a factor of two less than those of the mid–latitude and subtropical continental storms investigated in the Thunderstorm Project. Jorgensen *et al.* (1985) further showed that the peak draught intensities in cores in hurricanes were similar to those in the GATE MCSs examined by LeMone and Zipser.

Questions remain regarding whether the GATE flights sampled the most intense convection that occurs within oceanic tropical MCSs, whether the flight-level data examined by Jorgensen *et al.* were representative of the most intense vertical motions in hurricanes and whether draughts in the air-mass storms studied in the Thunderstorm Project are similar to the draughts in larger mid–latitude MCSs. However, these results are at present the best available statistical indicators of the scales and intensities of the individual draughts.

Prior to the writing of Houze (1982), it was thought that the convective downdraughts were primarily located in the lower troposphere and were the result of precipitation loading and evaporation into dry environmental air entrained at low to middle levels. However, upper-level downdraughts adjacent to the upper portions of intense convective updraughts have now been found in mid–latitude squall lines by Heymsfield and Schotz (1985) and Smull and Houze (1987). Recently, these upper-level downdraughts have been documented in several mid-latitude MCSs in the PRE-STORM program. An example dual-Doppler radar data analysis[1] showing a vertical motion pattern typical of the convective regions of these MCSs is shown in Fig. 20. The system was moving from left to right in this cross-section. A reflectivity core in the squall line is seen at $x = 20$ km. Three major updraught peaks are seen at progressively higher altitudes at $x = 30$, 20 and 13 km. A low-level downdraught is seen at $x = 17$ km. Upper-level downdraughts located between the updraughts are seen above the 8 km level at $x = 18$ and 21 km, immediately ahead of and behind the intense reflectivity cell.

(ii) *A mid–latitude continental case.* A mid–latitude MCS for which estimates of the mean vertical velocity in the convective region are available is the 22 May 1976 Oklahoma squall line, whose stratiform-region w profiles were illustrated in Fig. 18(a). The convective-region w profile in this storm (Fig. 21) was diagnosed from rawinsonde data by

[1] The dual-Doppler data were obtained with the National Center for Atmospheric Research (NCAR) CP-3 and CP-4 C-band radars located 60 km apart. The NCAR Research Data Support System (RDSS) software was used to edit the data. Interpolation of the data to a common Cartesian grid with a grid spacing of 1·5 km in the horizontal and 0·5 km in the vertical was carried out with the NCAR Sorted Position Radar Interpolation (SPRINT) software (Mohr *et al.* 1979). Winds were then derived by means of the NCAR Cartesian Editing and Display of Radar Data under Interactive Control (CEDRIC) (Mohr and Miller 1983). Vertical air motion (w) was computed by integrating the anelastic mass continuity equation downward. A boundary condition on w was applied at the height of the uppermost level at which divergence could be determined in CEDRIC. Wherever this height exceeded 13·5 km and the radar reflectivity factor exceeded 20 dBZ, the echo was considered to be a convective cell and a value of $w = 0{\cdot}25$ m/s was used. Otherwise, a value of $w = 0$ was used. Variation of these upper-level boundary values between 0 and 2 m/s in the convective cells and from 0 to 0·5 m/s elsewhere did not change the character of the results substantially. Nor did the addition of a constraint at the lower boundary (Biggerstaff *et al.* 1988).

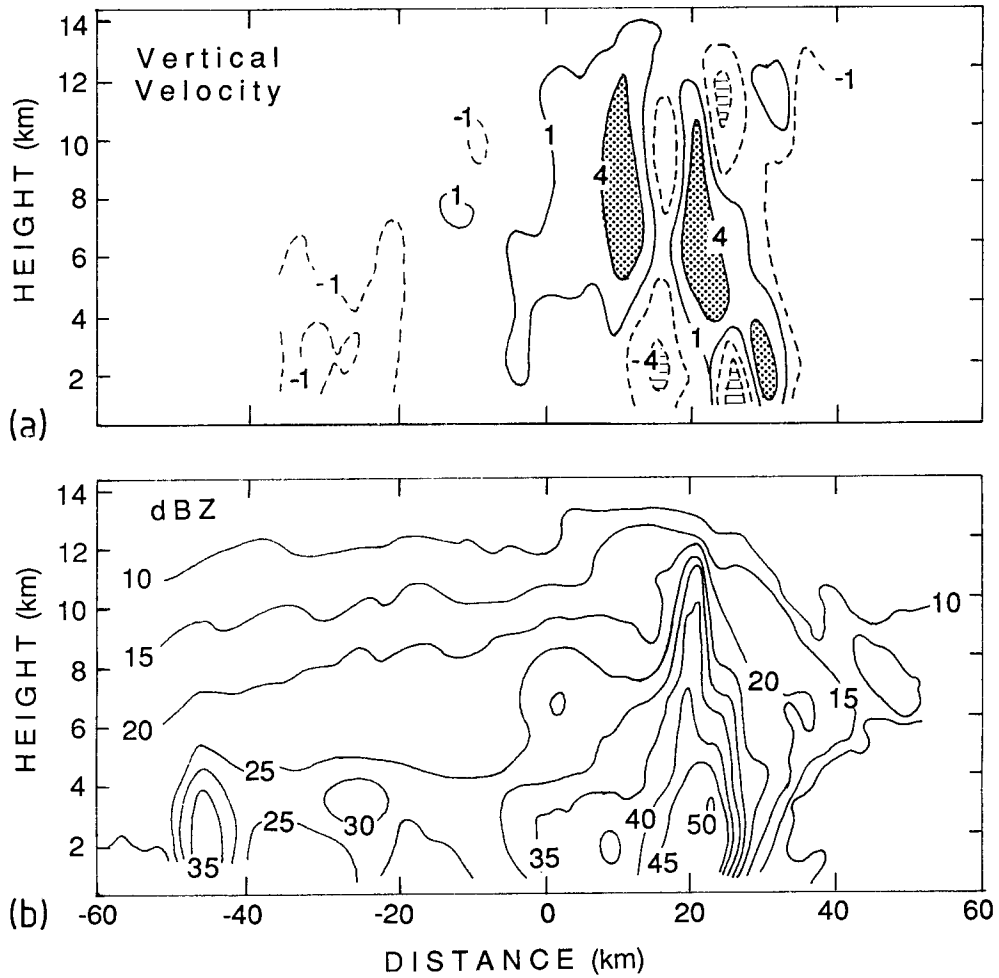

Figure 20. (a) Vertical velocities derived by dual-Doppler radar analysis for a representative cross-section through the convective region of the Kansas squall line of 11 June 1985 (see Fig. 13(a)). Contours in m/s. (b) Radar reflectivity (dBZ) for same cross-section.

Ogura and Liou (1980, curve OL) and from dual-Doppler radar data by Smull and Houze (1987, curve SH). The two curves exhibit similar shapes, particularly the sharp peak at about 3 km altitude. However, the maximum value (0·3–0·5 m/s) is considerably less than the typical peak values seen in individual draughts (e.g. Figs. 19 and 20). Although these two estimates are in reasonable agreement, they may both be underestimates. The Smull and Houze curve was computed for a portion of the region of radar reflectivity (i.e., precipitation) that had convective structure. Convective draughts that existed in developing clouds ahead of the band of precipitation were thus not included in the average. The updraughts in the developing clouds were probably quite intense, and their inclusion would probably have increased the areally-averaged w. The Ogura and Liou average was computed from a time–space composite of rawinsonde data. The rawinsonde data had relatively low resolution in time and space (compared with the radar data) and the compositing procedure has the effect of smoothing the wind field.

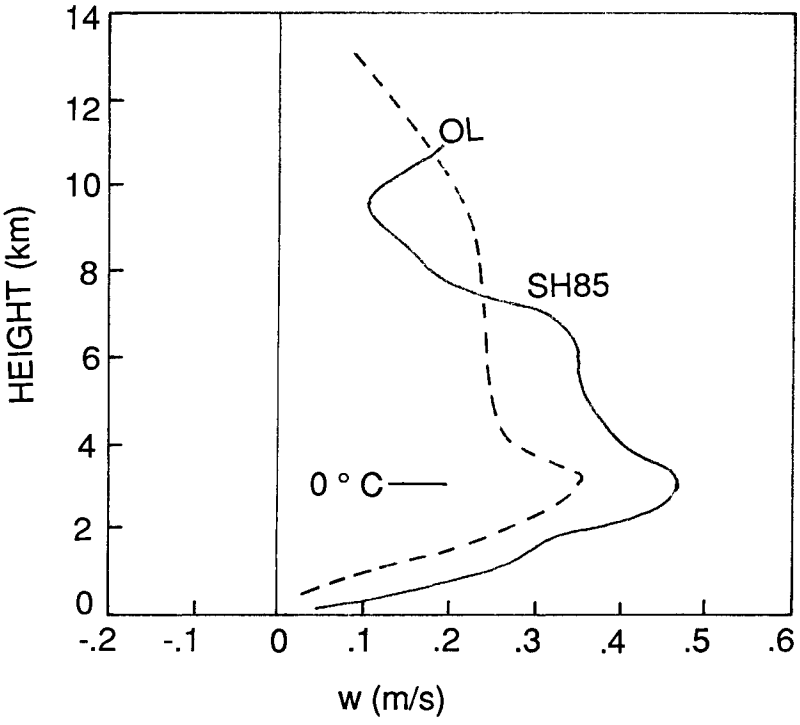

Figure 21. Convective-region vertical velocity profiles for the Oklahoma squall line of 22 May 1976. Curve OL is from Fig. 16 of Ogura and Liou (1980); data are from their $x = -22{\cdot}5$. Curve SH is from the dual-Doppler radar analysis of Smull and Houze (1987).

(iii) *Tropical oceanic island cases.* Composite analyses of ship rawinsondes and aircraft data taken in and near GATE squall line systems were performed by Gamache and Houze (1982, 1985) and Houze and Rappaport (1984). The stratiform-region w profiles for these two storms were shown in Fig. 16. The convective-region profiles are shown in Fig. 22. For the Gamache and Houze case (12 September 1974) three curves are shown. The GH82 AVE curve was derived from hand-analysed data for a $1{\cdot}5\times10^4\text{km}^2$ area containing the convective region. This region was considerably larger than the area of convective precipitation and was based on only eight levels of data. The GH82 PEAK curve was obtained from a contour analysis of the data at the location of the maximum w ($a = 25\,\text{km}$, $b = -25\,\text{km}$ in Fig. 15 of Gamache and Houze (1982)). The GH85 curve was obtained in a reanalysis of the composite wind field in the 12 September 1974 storm. The vertical resolution was improved, but the objective analysis of the composite fields evidently produced more smearing in the horizontal than did the hand analysis. The curve shown is an average for the same region as the GH82 AVE curve; however, lower values of w (by about a factor of three) were obtained for the GH85 curve.

The curve for the Houze–Rappaport case (28 June 1974) is indicated HR84 in Fig. 22. It was derived from hand analysis of composite wind data at five levels. The composite procedure and the low time and space resolution of the data probably both contributed to lowering the magnitude of the average w in the convective region. The curve obtained, however, is highly consistent with the GH82 and GH85 curves and with the profiles for the mid–latitude case in Fig. 21. The shapes of the GH85 and HR84 curves are remarkably similar.

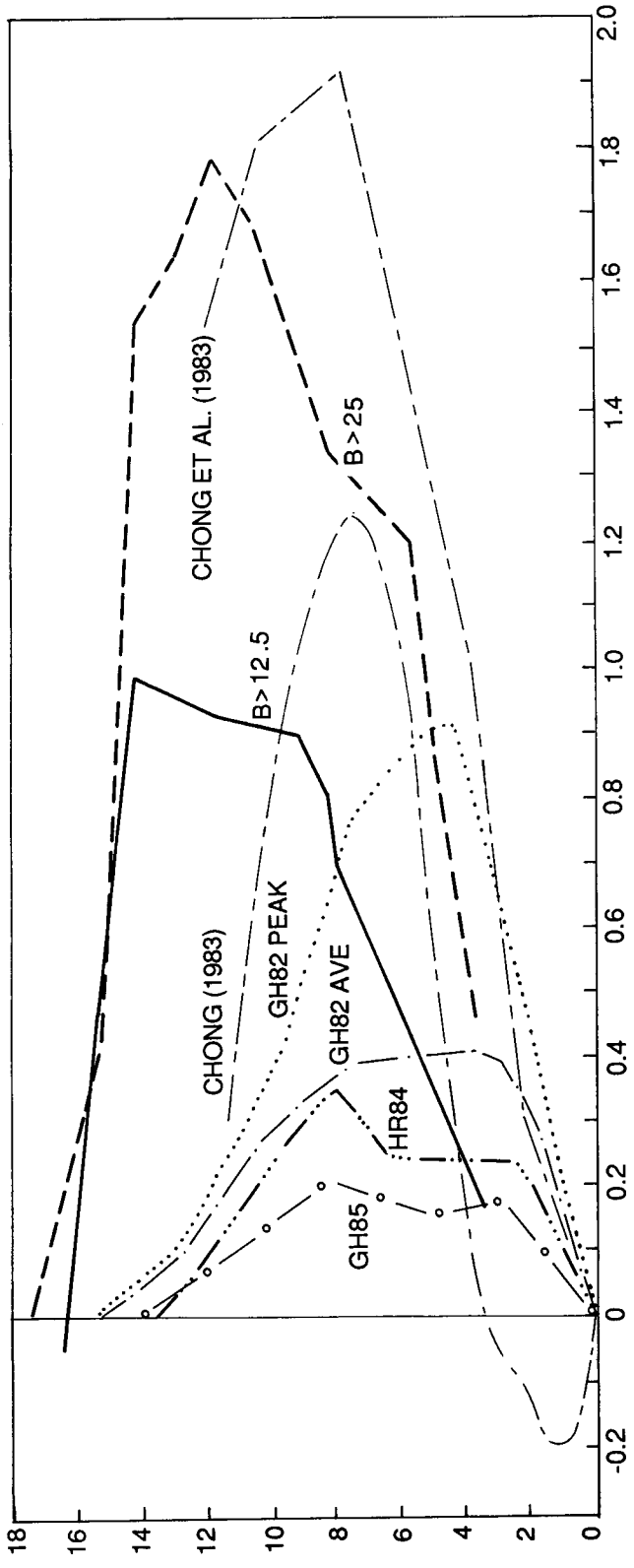

Figure 22. Convective-region vertical velocity profiles for tropical oceanic and island cases. Curve GH85 is from Gamache and Houze's (1985) objective analysis of the composite sounding and aircraft wind data for the 12 September 1974 GATE squall line. The GH82 AVE profile is Gamache and Houze's (1982) estimate for the same region based on subjectively analysed maps of the same data. The GH82 PEAK curve shows their analysed values at the location of the maximum w (a = 25 km, b = −25 km in Fig. 15 of Gamache and Houze 1982). Curve HR84 is from Houze and Rappaport's (1984) composite sounding and aircraft wind analysis of the 28 June 1974 GATE squall line. The curves labelled $B > 12{\cdot}5$ and $B > 25$ are from Balsley *et al.* (1988); they are the average profiler-detected vertical velocities for a two-year period at Pohnpei island in the western Pacific. The curves from Chong (1983) and Chong *et al.* (1983) are for the 22 June COPT '81 squall line.

(iv) *Tropical continental case.* Also shown in Fig. 22 are two convective-region vertical motion profiles for the 22 June 81 squall system observed over western Africa during COPT '81 (same storm for which the stratiform-region vertical profiles of vertical velocity are shown in Fig. 17). The profile from Chong *et al.* (1983) in Fig. 22 was obtained by dual-Doppler analysis and is averaged over a domain of $40\times40\,km^2$. The profile from Chong (1983) was obtained by single-Doppler VAD technique and is averaged over a circle 80 km in diameter. The peak velocities were greater and located at a higher altitude than those of the GATE curves shown in the same figure.

As noted above, the lower magnitudes of the GATE squall line convective-region w profiles in Fig. 22 (GH82, GH85 and HR84) and the Ogura–Liou (1980) mid–latitude squall line profile in Fig. 21 probably were a result of smearing inherent in the compositing procedure and low time and space resolution of the sounding and aircraft wind data. Therefore, the differences in intensity between these curves and radar- or profiler-derived curves are probably not meaningful. Probably more significant is the difference in the altitude at which the maximum areal-mean vertical velocity is observed. While it cannot be ruled out that the COPT '81 profiles are biased in shape because radar samples only in areas of precipitation, it is likely that this comparison indicates that the continental convection had a higher altitude of maximum vertical velocity.

(v) *Tropical island cases.* Mean convective-region vertical motion profiles obtained by Balsley *et al.* (1988) by averaging the Pohnpei profiler data for all the heavy rain occurrences in a two-year period are also shown in Fig. 22. Two categories of heavy rain occurrences were considered by Balsley *et al.*: those in which hourly rain accumulations exceeded 12·5 and 25 mm. The $B > 12{\cdot}5$ and $B > 25$ curves in Fig. 22 show the average profiles for these two rainfall thresholds. The magnitudes of the peak values of mean w in these profiles are 1 m/s for the 12·5 mm rain threshold and 1·8 m/s for the 25 mm threshold. Strong maxima of w are indicated in the high troposphere; both the magnitudes and the shapes of the profiles of w differ strongly from the GATE cases in Fig. 22 and the mid–latitude case in Fig. 21. However, the Balsley *et al.* profiles resemble the continental tropical (COPT '81) data, except that the maximum occurs at a still greater altitude.

The strong upper tropospheric maximum seen at 12–14 km in the Pohnpei profiler results ($B > 12{\cdot}5$ and $B > 25$ curves) suggests that these profiles represent one extreme of the spectrum of convective-region vertical profile types. The convection in the western Pacific may differ meteorologically from that over continental West Africa and from that in the eastern Atlantic, where the GATE data were obtained, because of differing environmental conditions. The thermodynamic structure of the environment is known to be somewhat more unstable in the western Pacific (Thompson *et al.* 1979). However, the low-level convective heating maximum found by Johnson (1984) for the western Pacific (section 2(*b*); Fig. 7) indicates maximum vertical velocity in the lower troposphere in convective regions of mesoscale cloud systems. Johnson's results thus appear to contradict those of Balsley *et al.* since Pohnpei lies on one corner of the same region of Pacific islands as that studied by Johnson. It is possible that the sampling by the Pohnpei profiler was biased in some subtle way toward periods when velocities were maximum at upper levels, so that a different profile applies over the island than over the entire region studied by Johnson. For example, the complex orography of the island of Pohnpei, which has several mountains 600–800 m high, may have produced a vertical motion regime in which the upper-level maximum was favoured.

The diversity of convective-region vertical profiles seen in Figs. 21 and 22 indicates that much remains to be done to clarify the nature of the vertical velocity in the convective regions of MCSs and how these profiles vary from one large-scale environment to another.

(c) *Consistency of observed vertical velocity profiles with large-scale heating profiles of the conceptual model MCS*

The conceptual model heating rates of Houze (1982) shown in Fig. 1 were calculated for a large-scale region over which an average of 3 cm/d of rain was falling. The magnitude of the vertical velocities used in Houze's calculations were directly proportional to this assumed rainfall rate. This amount of rain would, however, occur only in a very disturbed situation. When Johnson (1984) reassessed the western Pacific heating profile of Yanai *et al.* (1973), he estimated that the average rain rate for typical disturbed conditions in the region of the Intertropical Convergence Zone examined by Yanai *et al.* was 1·4 cm/d; however, for simplicity, he normalized his results (such as those in Fig. 7) to correspond to a 1 cm/d rain rate. In this section, we adopt 1·4 cm/d as a typical rain rate and renormalize both Johnson's (1984) and Houze's (1982) results to a rain rate of 1·4 cm/d.

(i) *Stratiform-region heating profile.* When the stratiform-region heating rates of Houze (1982) (Fig. 3(b)) and Johnson (1984) (Fig. 7) are normalized to a large-scale area rain rate of 1·4 cm/d, they have the values shown in Fig. 23 (curves H and J). This same comparison was shown in Fig. 6 by Johnson and Young (1983) using a different normalization scheme. As before, excellent agreement is seen. It was achieved primarily

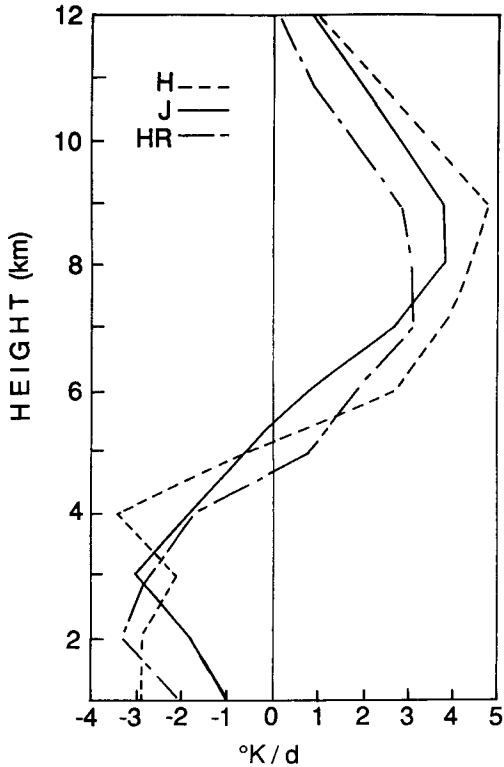

Figure 23. Mean heating rate in stratiform regions of mesoscale convective systems. Curve H shows non-radiative heating rate computed by Houze (1982) normalized to a large-scale average rain rate of 1·4 cm/d. Curve J shows Johnson's (1984) mesoscale stratiform heating rate normalized to a large-scale average rain rate of 1·4 cm/d. Curve HR is a recomputation of Houze's (1982) net stratiform-region heating by condensation and evaporation with Houze and Rappaport's (1984) diagnosed stratiform-region vertical motion (curve HRSF in Fig. 16) substituted for Houze's (1982) stratiform-region vertical motion estimate based on rain amount and a simple cumulus model.

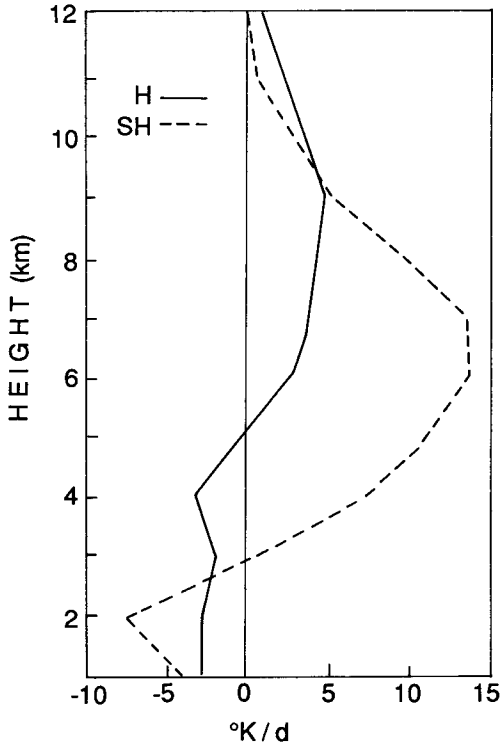

Figure 24. Comparison of Houze's (1982) mean stratiform-region heating rate (curve H) with the heating rate in a small sub-region of the stratiform region of the mid-latitude squall line system (curve SH). Curve H is the same as in Fig. 23. Curve SH is from the dual-Doppler radar analysis of Smull and Houze (1987).

because the vertical motion profile diagnosed by Johnson (1982) from Winter MONEX sounding data (Fig. 16) was consistent with the vertical velocity profile assumed by Houze (1982) for the stratiform region.

The similarity of the other oceanic tropical mean stratiform-region vertical motion profiles shown in Fig. 16 to that of the Johnson (1982) profile indicates that these profiles also produce heating rates similar to the Houze (1982) heating profile. The HR profile shown in Fig. 23 illustrates this point. Since the mesoscale condensation and evaporation in the stratiform region (term (iii) in Eq. (1)) dominate the diabatic heating in the stratiform region, this term can alone be used to estimate the stratiform-region heating profile. This term in the Houze stratiform-region heating profile (Fig. 3(b)) was recomputed with Houze and Rappaport's (1984) stratiform-region vertical velocity profile (in Fig. 16) substituted for the vertical velocity profile used in Houze (1982). The result is the HR profile in Fig. 23. This curve is very similar to the Houze (1982) and Johnson (1984) stratiform-region heating profiles.

Figures 17 and 18 show that at specific locations in the stratiform regions of continental tropical and mid-latitude squall line MCSs the vertical velocity is a factor of 2 to 4 greater than in the average profiles for tropical oceanic and island stratiform areas (Fig. 16). The corresponding difference in heating rate is illustrated in Fig. 24, where the Houze stratiform-region heating is compared with a profile (labelled SH) given by term (iii) in Eq. (1) recomputed by substituting the dual-Doppler radar vertical velocity profile obtained by Smull and Houze (1987) in the stratiform region of a mid-latitude squall line MCS (curve SH2 in Fig. 18(a)) for the vertical velocity profile used in Houze (1982).

(ii) *Convective-region heating profile.* When the convective-region heating profiles of Houze (1982) and Johnson (1984) from Figs. 3(a) and 7 are normalized to a 1·4 cm/d rain rate and compared, the result in Fig. 25 is obtained. The magnitudes of the maximum heating rates are similar; however, the peak convective heating is found at a lower altitude by Johnson. As noted in section 2(*b*), this difference in the vertical profile of heating may be associated with the inclusion of the effects of smaller cumulus in Johnson's estimate but might also result from Houze's assumption of a weakly entraining jet to represent the vertical velocity profile. Neither Johnson's nor Houze's convective-region heating profiles are based on observations of convective-region vertical velocities. The shape of Houze's w profile was assumed. Johnson's profile was deduced as a residual from other observationally-based profiles.

Observations of winds in and near convective regions of squall line MCSs were used by Smull and Houze (1987), Houze and Rappaport (1984) and Gamache and Houze (1985) to obtain the convective-region vertical profiles labelled SH, HR84 and GH85, respectively, in Figs. 21 and 22. The convective-region heating profile of Houze (1982) was recalculated by substituting these heating profiles into term (ii) of Eq. (1) in place of the vertical velocity used by Houze (1982) and using this term alone to estimate the total convective heating profile. (This estimate could be in significant error if term (v) in Eq. (1) is more important than previously thought as a result of the upper-level downdraught activity noted in section 4(*b*)(i)). The recalculated profiles, labelled SH, HR and

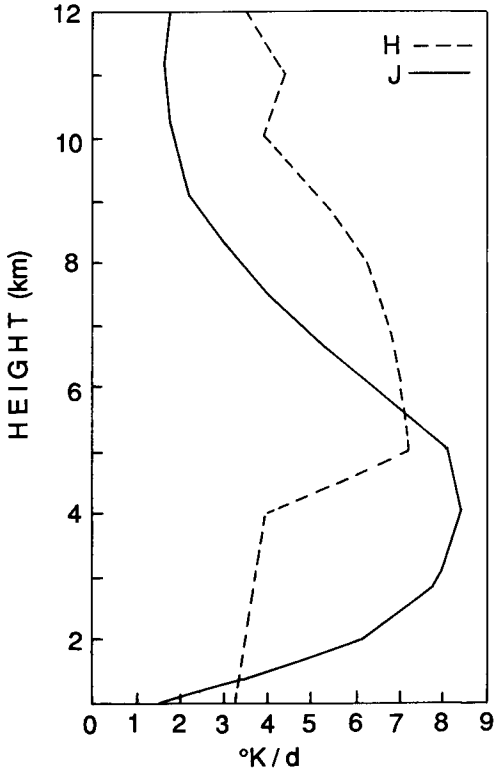

Figure 25. Indirect estimates of heating rate in convective regions of mesoscale convective systems. Curve H shows heating rate estimated by Houze (1982) using rain amount and a simple cumulus model. His values are normalized to a large-scale average rain rate of 1·4 cm/d. Curve J shows Johnson's (1984) convective heating rate obtained as a residual of total heating inferred from large-scale sounding data and stratiform region heating profiles. His values are also normalized to a large-scale average rain rate of 1·4 cm/d.

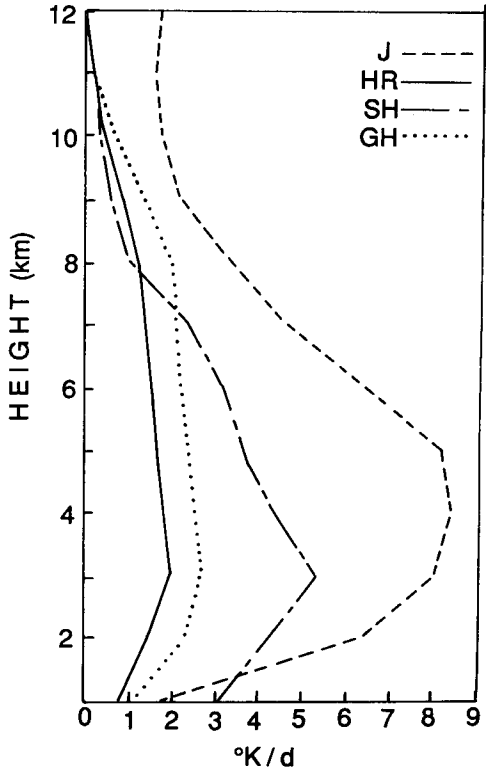

Figure 26. Johnson's (1984) indirect estimate of the convective heating rate (curve J, same as in Fig. 25) compared with heating rates computed from three different observed convective-region vertical motion profiles. Profile SH is a recomputation of Houze's (1982) net convective-region heating by condensation and evaporation with Smull and Houze's (1987) convective-region vertical motion profile derived from dual-Doppler radar analysis (Fig. 21) substituted for Houze's (1982) convective-region vertical motion estimate based on rain amount and a simple cumulus model. Profiles GH and HR are similar recomputations using Houze and Rappaport's (1984) diagnosed convective-region vertical motion (curve HR84 in Fig. 22) and Gamache and Houze's (1985) diagnosed convective-region vertical motion (curve GH85 in Fig. 22).

GH, are compared with Johnson's (1984) profile (labelled J) in Fig. 26. All three of these observationally based profiles suggest a lower tropospheric maximum of heating, similar to Johnson's (1984) profile.

As noted in section 4(*b*)(v), the tropical island data of Balsley *et al.* (1988) are characterized by a strong upper-level maximum of average vertical velocity in intense rain situations, as are the continental tropical profiles of Chong (1983) and Chong *et al.* (1983). To examine the implications of this type of profile for large-scale heating, term (v) in Eq. (1) has been recomputed using the extreme profile of Balsley *et al.* (curve $B > 25$ in Fig. 22) in place of the vertical velocity used by Houze (1982). The result is shown in Fig. 27 in comparison with the convective-region curve of Houze (normalized to a rain rate of 1·4 cm/d). The shape of the curve is quite similar to the Houze curve. However, the significance and interpretation of this result are not clear. The shape of the Houze curve was based on the assumption of a weakly entraining jet model. The Johnson (1984) profile and the three observationally based profiles in Fig. 26, which involve no such assumption, all suggest a lower tropospheric profile, at least in the large-scale settings that they represent. Because of these uncertainties any conclusions regarding the vertical profiles of heating associated with the convective regions of MCSs must be very tentative. However, if all the data sets reviewed here are accepted as reasonably

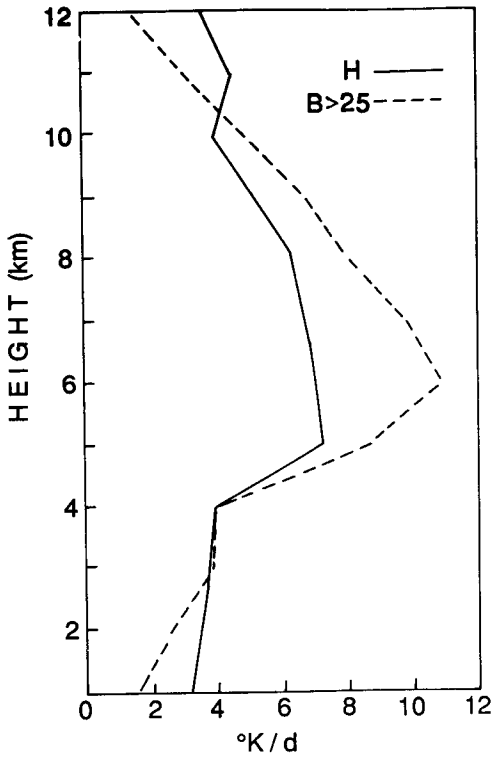

Figure 27. Comparison of Houze's (1982) estimate of convective heating rate (curve H, same as in Fig. 25) with heating rate computed from the profiler-observed vertical motion of Balsley *et al.* (1988) for heavy rain conditions on Pohnpei (rain rates over 25 mm/h). Profile $B > 25$ is computed in the same way as profiles SH, GH and HR in Fig. 26, except that curve $B > 25$ in Fig. 22 is the one substituted for Houze's (1982) convective-region vertical motion estimate based on rain amount and a simple cumulus model.

accurate, albeit they were obtained and analysed in different ways, it would appear that the level at which the maximum heating occurs as a result of the vertical motion in the convective regions of MCSs varies considerably, from the low troposphere, as in the GATE cases, to the very high troposphere, as suggested by the Pohnpei and West African data.

5. Conclusions

During the last five years, the conceptual model of an MCS presented by Houze (1982) has been confirmed and refined. As he proposed, the mesoscale convective systems responsible for most tropical rainfall exhibit a structure in which regions of deep convection are accompanied by mesoscale stratiform precipitation areas. The stratiform cloud is based in the mid-troposphere and contains a mesoscale updraught, while mesoscale subsidence occurs below the cloud base. Ice particles detrained or left aloft by the deep convective towers are advected horizontally into the stratiform cloud by storm-relative winds and grow through deposition of water vapour condensed in the mesoscale updraught. The ice particles melt into raindrops that partially evaporate in the region of subsidence below the stratiform cloud base.

This type of precipitation structure is also seen in the MCSs that produce much of the warm season rainfall over the continental United States and in hurricanes, which account for a significant proportion of tropical rainfall.

The horizontal configurations and arrangements of the convective and stratiform precipitation areas vary. However, large areas of stratiform rain are typically found adjacent to convective areas, and vertical cross-sections similar to Fig. 2 generally apply.

The net heating of the large-scale environment by an MCS is the combined effect of the heating by the convective and stratiform components of the system. Houze (1982) demonstrated that this heating is determined largely by the condensation and evaporation associated with the vertical air motions in the convective and stratiform regions. Melting of snow in the stratiform region and radiative flux convergence also contribute significantly to the net heating but are not dealt with in this paper. Recent observational evidence on the vertical profiles of vertical motion in the convective and stratiform regions of MCSs has been reviewed here to determine its consistency or otherwise with the convective and stratiform heating profiles hypothesized by Houze (1982).

Data on vertical motion profiles in the stratiform regions of oceanic-tropical, tropical-island, continental-tropical and mid-latitude-continental MCSs all agree rather well with the stratiform-region w profiles assumed by Houze (1982). Upward motion, with a maximum of 10–50 cm/s, occurs in the upper troposphere. Mesoscale subsidence of similar intensity occurs in the lower troposphere. The level of zero vertical air motion, assumed by Houze to occur at the 0 °C level, actually occurs at or slightly above the 0 °C level. The height of the $w = 0$ level can vary within a single storm from 0 to 2 km above the 0 °C level. This height is determined, at least in some cases, by the depth of dry air layers that flow into the stratiform region. Thus, the depth of the subsidence layer in the stratiform region appears actually to be somewhat greater than assumed in Houze. Since this subsidence constitutes the evaporational cooling layer of the stratiform region, which reduces the net heating of the large-scale environment by the MCS at lower levels (Figs. 3(b) and 5), it appears that this reduction of the net heating occurs through a slightly deeper layer than previously thought.

Data on vertical motion profiles in the convective regions of MCSs show more variation from study to study than do the observations of stratiform-region vertical motions. It is difficult to determine whether the differences in estimates are meteorological, arise from different types of observations, are the result of different analysis methods or are the result of different sampling strategies. The largest differences in convective-region vertical profiles of vertical motion are seen in the middle to upper troposphere, where there is considerable variation in both magnitude and shape of the vertical profile among the various estimates, particularly with regard to the level at which the maximum mean vertical velocity occurs. This level ranges from 3 to 12 km. In future observational studies, particular attention should be paid to clarifying the magnitude and vertical distribution of mean vertical velocity in convective regions of MCSs and the variation of these vertical profiles from one synoptic setting to another.

The various data on vertical motion profiles have been examined for their consistency with the hypothesized heating profiles of Houze (1982). The mean stratiform-region vertical velocity profiles observed in tropical oceanic and island cloud systems consistently produce heating profiles very similar to the stratiform-region profile estimated by Houze: heating at upper levels and cooling at lower levels, where the mesoscale subsidence occurs. However, a variety of results has emerged for the convective regions, as a result of the various vertical motion profiles that have been obtained: some observational studies indicate a maximum of convective heating in the low troposphere, while others indicate a mid-tropospheric heating maximum.

The ubiquitous occurrence of stratiform regions in MCSs and hurricanes, together with their consistent heating profiles, which systematically concentrate heating in upper levels while cooling lower levels, indicate that these stratiform regions are a major consideration in evaluating the interaction of mesoscale systems with the large-scale environment. As indicated by Houze (1982), the effect of these stratiform regions is to lead to more heating of the environment in the upper troposphere and less in the lower troposphere than would be the case if the precipitation was all convective in nature. However, the consistency of the stratiform profiles from case to case indicates that the variability of net (convective plus stratiform) heating profiles from case to case lies primarily in the variation of the convective-region profiles from one case to another. Future work should therefore be focused on the variation of the convective-region profiles from one large-scale situation to the next and on the environmental factors controlling these changes.

Finally, it is noted that in this paper we have considered only the heating profile associated with the profile of the areal mean of w. However, the recent Doppler radar studies that indicate the presence of upper-level downdraughts in the convective regions of MCSs suggest that future studies should also assess the impact of these downdraughts on the profiles of mean w in convective regions and on the eddy flux convergence (term (v) in Eq. (1)). Owing to these downdraughts, this term may be larger in the upper troposphere than thought at the time of writing of the Houze (1982) paper.

Acknowledgements

The author benefited from discussions with R. H. Johnson, B. B. Balsely, B. F. Smull and S. A. Rutledge and from reviewers' comments. PRE-STORM and EMEX data and analyses were provided by M. I. Biggerstaff, S. A. Rutledge, B. Mapes and S. Bograd. This work was supported by the National Science Foundation under grants ATM-8413546 and ATM-8616647, the National Oceanic and Atmospheric Administration Hurricane Research Division under grant 40-WCNR-6-02428 and the National Aeronautics and Space Administration under grant NAG5-784.

References

Atlas, D., Hardy, K. R., Wexler, R. and Boucher, R. J. 1963 On the origin of hurricane spiral bands. *Geofis. Int.*, **3**, 123–132

Balsley, B. B., Ecklund, W. L., Carter, D. A., Riddle, A. C. and Gage, K. S. 1988 Average vertical motions in the tropical atmosphere observed by a radar wind profiler on Pohnpei (7 °N latitude, 157 °E longitude). *J. Atmos. Sci.*, **45**, 396–405

Barnes, G. M. and Sieckman, K. 1984 The environment of fast- and slow-moving tropical mesoscale convective cloud lines. *Mon. Weather Rev.*, **112**, 1782–1794

Biggerstaff, M. I., Houze, R. A., Jr. and Rutledge, S. A. 1988 'Vertical drafts in the convective regions of mesoscale convective systems in Kansas'. Pp. 705–707 in preprints *Tenth International Cloud Physics Conference*, Bad Homburg, 15–20 August 1988. Duetscher Wetterdienst

Browning, K. A. and Wexler, R. 1968 The determination of kinematic properties of a wind field using Doppler radar. *J. Appl. Meteorol.*, **7**, 105–113

Byers, H. R. and Braham, R. R., Jr. 1949 *The Thunderstorm*. U.S. Government Printing Office, Washington, U.S.A.

Chong, M. 1983 'Les radars météorologiques Doppler pour l'étude de la convection orgeuse. Application à une ligne de grains tropicale'. Thése de Doctorat d'Etat. Université de Paris, France

Chong, M., Testud, J. and Roux, F. 1983 Three-dimensional wind field analysis from dual-Doppler radar data. Part II: Minimizing the error due to temporal variation. *J. Clim. Appl. Meteorol.*, **22**, 1216–1226

Chong, M., Amayenc, P., Scialom, G. and Testud, J. 1987 A tropical squall line observed during the COPT 81 experiment in West Africa. Part I: Kinematic structure inferred from dual-Doppler radar data. *Mon. Weather Rev.*, **115**, 670–694

Churchill, D. D. and Houze, R. A., Jr. 1984 Development and structure of winter monsoon cloud clusters on 10 December 1978. *J. Atmos. Sci.*, **41**, 933–960

DeMaria, M. 1985 Linear response of a stratified tropical atmosphere to convective forcing. *ibid.*, **42**, 113–121

Drosdowsky, W. 1984 Structure of a northern Australian squall line system. *Aust. Meteorol. Mag.*, **32**, 177–183

Fritsch, J. M. and Maddox, R. A. 1981a Convectively driven mesoscale weather systems aloft. Part I. Observations. *J. Appl. Meteorol.*, **20**, 9–19

1981b Convectively driven mesoscale weather systems aloft. Part II. Numerical simulations. *ibid.*, **20**, 20–26

Fritsch, J. M., Kane, R. J. and Chelius, C. R. 1986 The contribution of mesoscale convective weather systems to the warm-season precipitation in the U.S. *J. Clim. Appl. Meteorol.*, **25**, 1333–1345

Fujita, T. T. 1955 Results of detailed synoptic studies of squall lines. *Tellus*. **7**, 405–436

Gamache, J. F. and Houze, R. A., Jr. 1982 Mesoscale air motions associated with a tropical squall line. *Mon. Weather Rev.*, **110**, 118–135

1983 Water budget of a mesoscale convective system in the tropics. *J. Atmos. Sci.*, **40**, 1835–1850

1985 Further analysis of the composite wind and thermodynamic structure of the 12 September GATE squall line. *Mon. Weather Rev.*, **113**, 1241–1259

Godbole, R. V. 1977 The composite structure of the monsoon depression. *Tellus*. **29**, 25–40

Hamilton, R. A. and Archbold, J. W. 1945 Meteorology of Nigeria and adjacent territory. *Q. J. R. Meteorol. Soc.*, **83**, 303–314

Hartmann, D. L., Hendon, H. H. and Houze, R. A., Jr. 1984 Some implications of the mesoscale circulations in tropical cloud clusters for large-scale dynamics and climate. *J. Atmos. Sci.*, **41**, 113–121

Heymsfield, G. M. and Schotz, S. 1985 Structure and evolution of a severe squall line over Oklahoma. *Mon. Weather Rev.*, **113**, 1563–1589

Houze, R. A., Jr. 1977 Structure and dynamics of a tropical squall-line system. *Mon. Weather Rev.* **105**, 1540–1567

1982 Cloud clusters and large-scale vertical motions in the tropics. *J. Meteorol. Soc. Jap.*, **60**, 396–410

1989 'Convective and stratiform precipitation in the tropics'. *Proceedings, international symposium on tropical precipitation measurements.* Tokyo, Japan. Science and Technology Corp., Hampton, VA (in press)

Houze, R. A., Jr. and Betts, A. K. 1981 Convection in GATE. *Rev. Geophys. Space Phys.*, **19**, 541–576

Houze, R. A., Jr. and Churchill, D. D. 1987 Mesoscale organization and cloud microphysics in a Bay of Bengal depression. *J. Atmos. Sci.*, **44**, 1845–1867

Houze, R. A., Jr. and Rappaport, E. N. 1984 Air motions and precipitation structure of an early summer squall line over the eastern tropical Atlantic. *ibid.*, **41**, 553–574

Houze, R. A., Jr., Geotis, S. G., Marks, F. D., Jr. and West, A. K. 1981 Winter monsoon convection in the vicinity of north Borneo. Part I: Structure and time variation of the clouds and precipitation. *Mon. Weather Rev.*, **109**, 1595–1614

Johnson, R. H. 1982 Vertical motion of near-equatorial winter monsoon convection. *J. Meteorol. Soc. Jap.*, **60**, 682–690

1984 Partitioning tropical heat and moisture budgets into cumulus and mesoscale components: Implications for cumulus parameterization. *Mon. Weather Rev.*, **112**, 1590–1601

1986 Lower-tropospheric warming and drying in tropical mesoscale convective systems: implications for the problem of cumulus parameterization. *J. Meteorol. Soc. Jap.*, **64**, 721–726

Johnson, R. H. and Hamilton, P. J.	1988	The relationship of surface pressure features to the precipitation and air flow structure of an intense midlatitude squall line. *Mon. Weather Rev.*, **116**, 1444–1472
Johnson, R. H. and Houze, R. A., Jr.	1987	'Precipitating cloud systems of the Asian monsoon'. Pp. 298–353 in *Monsoon meteorology*. C.-P. Chang and T. N. Krishnamurti, Eds. Oxford University Press, New York
Johnson, R. H. and Nicholls, M. E.	1983	A composite analysis of the boundary layer accompanying a tropical squall line. *Mon. Weather Rev.*, **111**, 308–319
Johnson, R. H. and Young, G. S.	1983	Heat and moisture budgets of tropical mesoscale and clouds. *J. Atmos. Sci.*, **40**, 2138–2147
Jorgensen, D. P., Zipser, E. J. and LeMone, M. A.	1985	Vertical motions in intense hurricanes, *ibid.*, **42**, 839–856
Leary, C. A. and Houze, R. A., Jr.	1979a	The structure and evolution of convection in a tropical cloud cluster, *ibid.*, **36**, 437–457
	1979b	Melting and evaporation of hydrometeors in precipitation from anvil clouds of deep tropical convection. *ibid.*, **36**, 669–679
LeMone, M. A. and Zipser, E. J.	1980	Cumulonimbus vertical velocity events in GATE. Part I: Diameter, intensity and mass flux. *ibid.*, **37**, 2444–2457
LeMone, M. A., Barnes, G. M. and Zipser, E. J.	1984	Momentum flux by lines of cumulonimbus over the tropical oceans. *ibid.*, **41**, 1914–1932
Maddox, R. A.	1980	An objective technique for separating macroscale and mesoscale features in meteorological data. *Mon. Weather Rev.*, **108**, 1108–1121
	1981	'The structure and life cycle of mid-latitude mesoscale convective complexes'. Atmos. Sci. Pap. No. 336. Colorado State University, Ft Collins
Maddox, R. A., Perkey, D. J. and Fritsch, J. M.	1981	Evolution of upper tropospheric features during the development of a mesoscale convective complex. *J. Atmos. Sci.*, **38**, 1664–1674
Marks, F. D., Jr. and Houze, R. A., Jr.	1987	Inner core structure of hurricane Alicia from airborne Doppler radar observations. *J. Atmos. Sci.*, **44**, 1296–1317
Mohr, C. G. and Miller, L. J.	1983	CEDRIC—'A software package for Cartesian space editing, synthesis and display of radar fields under interactive control'. Pp. 559–574 in Preprints, 21st Conf. on Radar Meteorology, 19–23 September 1983, Edmonton, Alta., Canada. American Meteorological Society
Mohr, C. G., Miller, L. J. and Vaughn, R. L.	1979	An economical procedure for Cartesian interpolation and display of reflectivity factor data in three-dimensional space. *J. Appl. Meteorol.*, **18**, 661–670
Newton, C. W.	1950	Structure and mechanisms of the prefrontal squall line. *J. Meteorol.*, **7**, 210–222
Newton, C. W. and Fankhauser, J. C.	1964	On the movements of convective storms, with emphasis on size discrimination in relation to water-budget requirements. *J. Appl. Meteorol.*, **3**, 651–688
Ninomiya, K.	1971a	Dynamical analysis of outflow from tornado-producing thunderstorms as revealed by ATS III pictures. *ibid.*, **10**, 275–294
	1971b	Mesoscale modification of synoptic situations from thunderstorm development as revealed by ATS III and aerological data. *ibid.*, **10**, 1103–1121
Ogura, Y. and Liou, M. T.	1980	The structure of a midlatitude squall line. *J. Atmos. Sci.*, **37**, 553–567
Pedgley, D. E.	1962	*A meso-synoptic analysis of the thunderstorms on 28 August 1958.* Geophys. Mem., **106**. Meteorological Office
Ramage, C. S.	1971	*Monsoon meteorology*. Academic Press, New York
Rao, Y. P.	1976	*Southwest monsoon.* Meteorological Monograph. Synoptic Meteorology No. 1/1976. Indian Department of Meteorology, New Delhi
Riehl, H. and Malkus, J. S.	1958	On the heat balance in the equatorial trough zone. *Geophysica*, **6**, 503–538
Roux, F.	1987	'Les lignes de grains de COPT 81; Environnement, precipitations, cinematique et thermodynamique'. Ph.D. thesis, University of Paris, France
Rutledge, S. A. and Houze, R. A., Jr.	1987	A diagnostic modeling study of the trailing stratiform region of a midlatitude squall line. *J. Atmos. Sci.*, **44**, 2640–2656

Rutledge, S. A. and MacGorman, D. R. 1988 Cloud-to-ground lightning in the 10–11 June 1985 mesoscale convective system observed during O.K. PRE-STORM. *Mon. Weather Rev.*, **116,** 1393–1408

Rutledge, S. A., Houze, R. A., Jr., Biggerstaff, M. I. and Matejka, T. 1988 The Oklahoma–Kansas mesoscale convective system of 10–11 June 1985: Precipitation structure and single-Doppler radar analysis. *ibid.*, **116,** 1409–1430

Sanders, F. 1984 Quasi-geostrophic diagnosis of the monsoon depression of 5–8 July, 1979. *J. Atmos. Sci.*, **41,** 538–552

Simpson, R. H. and Simpson, J. 1966 Why experiment on tropical hurricanes? *Transactions of the New York Academy of Sciences*, Series II, **28,** 1045–1062

Smull, B. F. and Houze, R. A., Jr. 1985 A midlatitude squall line with a trailing region of stratiform rain: radar and satellite observations. *Mon. Weather Rev.*, **113,** 117–133

1987 Dual-Doppler radar analysis of a midlatitude squall line with a trailing region of stratiform rain. *J. Atmos. Sci.*, **44,** 2128–2148

Sommeria, G. and Testud, J. 1984 COPT 81: A field experiment designed for the study of dynamics and electrical activity of deep convection in continental tropical regions. *Bull. Am. Meteorol. Soc.*, **65,** 4–10

Srivastava, R. C., Matejka, T. J. and Lorello, T. J. 1986 Doppler radar study of the trailing anvil region associated with a squall line. *J. Atmos. Sci.*, **43,** 356–377

Thompson, R. M., Jr., Payne, S. W., Recker, E. E. and Reed, R. J. 1979 Structure and properties of synoptic-scale wave disturbances in the intertropical convergence zone of the eastern Atlantic. *ibid.*, **36,** 53–72

Warner, C. 1984 Core structure of a Bay of Bengal monsoon depression. *Mon. Weather Rev.*, **112,** 137–152

Warner, C. and Grumm, R. H. 1984 Cloud distributions in a Bay of Bengal monsoon depression. *ibid.*, **112,** 153–172

Warner, C., Simpson, J., van Helvoirt, G., Martin, D. W., Suchman, D. and Austin, G. L. 1980 Deep convection on day 261 of GATE. *ibid.*, **108,** 169–194

Webster, P. J. and Stephens, G. L. 1980 Tropical upper-tropospheric extended clouds: Inferences from Winter MONEX. *J. Atmos. Sci.*, **37,** 1521–1541

Wei, T. and Houze, R. A., Jr. 1987 The GATE squall line of 9–10 August 1974. *Adv. Atmos. Sci.*, **4,** 85–92

Williams, M. and Houze, R. A., Jr. 1987 Satellite-observed characteristics of winter monsoon cloud clusters. *Mon. Weather Rev.*, **115,** 505–519

Yanai, M., Esbensen, S. and Chu, J. H. 1973 Determination of bulk properties of tropical cloud clusters from large-scale heat and moisture budgets. *J. Atmos. Sci.*, **30,** 611–627

Zipser, E. J. 1969 The role of organized unsaturated convective downdraughts in the structure and rapid decay of an equatorial disturbance. *J. Appl. Meteorol.*, **8,** 799–814

1977 Mesoscale and convective-scale downdraughts as distinct components of squall-line circulation. *Mon. Weather Rev.*, **105,** 1568–1589

Zipser, E. J. and LeMone, M. A. 1980 Cumulonimbus vertical velocity events in GATE. Part II: Synthesis and model core structure. *J. Atmos. Sci.*, **37,** 2458–2469